POLITECNICO DI TORINO

Master's Degree Programme in Aerospace Engineering

Master's Thesis

Development and simulation of a supersonic aircraft model in a commercial flight simulation environment for future environmental impact reduction

Supervisor
Prof. Roberta FUSARO

Co-supervisor:
Oscar GORI

Candidate
Sara PALADINI
316572

Company Supervisors
Eng. Kiumars ASKARI - ENV-ISA

December 11, 2025

ABSTRACT

The thesis analysed a supersonic aircraft, part of the MOREandLESS project of the Politecnico di Torino, with the aim of assessing its acoustic and environmental impact during take-off and landing phases and optimising vertical flight profiles to reduce noise and emissions. The work was based on a supersonic aircraft model, with characteristics similar to the Concorde, developed in Plane Maker, and simulations were carried out in X-Plane integrated with neural networks and environmental models to estimate noise and emissions under different operating conditions. Standard emission models, including the Boeing Fuel Flow Method 2 (BFFM2) for pollutants, and main noise regulations were used as a reference for evaluating the optimised profiles. The results obtained provide a preliminary framework that will help guide future studies and support the development of strategies for sustainable supersonic aircraft design.

La tesi ha analizzato un velivolo supersonico, parte del progetto MOREandLESS del Politecnico di Torino, con l'obiettivo di valutarne l'impatto acustico e ambientale nelle fasi di decollo e atterraggio e di ottimizzare i profili verticali di volo per ridurre rumore ed emissioni. Il lavoro si è basato su un modello di velivolo supersonico, con caratteristiche simili al Concorde, sviluppato in Plane Maker e le simulazioni sono state svolte sul software X-Plane integrato con reti neurali e modelli ambientali per stimare rumore ed emissioni in diverse condizioni operative. Sono stati impiegati modelli standard di emissione, inclusa la metodologia Boeing Fuel Flow Method 2 (BFFM2) per gli inquinanti, e le principali normative sul rumore come riferimento per la valutazione dei profili ottimizzati. I risultati ottenuti offrono un quadro preliminare utile a orientare studi futuri e a supportare lo sviluppo di strategie per una progettazione sostenibile dei velivoli supersonici.

Contents

List of Tables

List of Figures

Chapter 1

INTRODUCTION

1.1 CONTEXT

Civil aviation is a continuously growing sector, driven by the increase in demand for air transport, international tourism, and the globalization of trade flows. This has led to significant economic and social benefits, but also to a significant increase in environmental impact, both globally, mainly through greenhouse gas emissions, and locally, through noise and air pollution in the vicinity of airports.
According to ICAO, the aviation sector contributes approximately 2% of global CO_2 emissions and, in the absence of corrective measures, air traffic is expected to double by 2050 [1]. Each kilogram of kerosene burned generates approximately 3.16 kg of CO_2, and emissions vary by flight category: approximately two-thirds of global kerosene consumption, and consequently CO_2 emissions, is due to short- and medium-range flights, which represent the majority of the global fleet, while regional flights contribute less than their numbers would suggest. [Fig. 1.1]

Among the various phases of flight, the terminal phases of takeoff and landing (LTO) are particularly critical because aircraft operate at low altitudes, close to the communities, consuming high amounts of fuel and generating significantly higher concentrations of emissions and noise levels than during cruise phases.

The main species emitted by engines during LTO phases include carbon dioxide (CO_2), water vapor (H_2O), nitrogen oxides (NO_x), carbon monoxide (CO), unburned hydrocarbons (HC), particulate matter (including soot and nvPM), and sulfur oxides (SO_x). Their distribution depends heavily on altitude and flight phase [Fig. 1.4]: at low altitudes, the effects on local air quality prevail, with increases in NO_2, formation of photochemical ozone and secondary particulate matter, while at high altitudes, radiative forcing, microphysical and photochemical effects (contrails and induced cirrus clouds) and O_3–CH_4 cycles linked to NO_x become relevant.

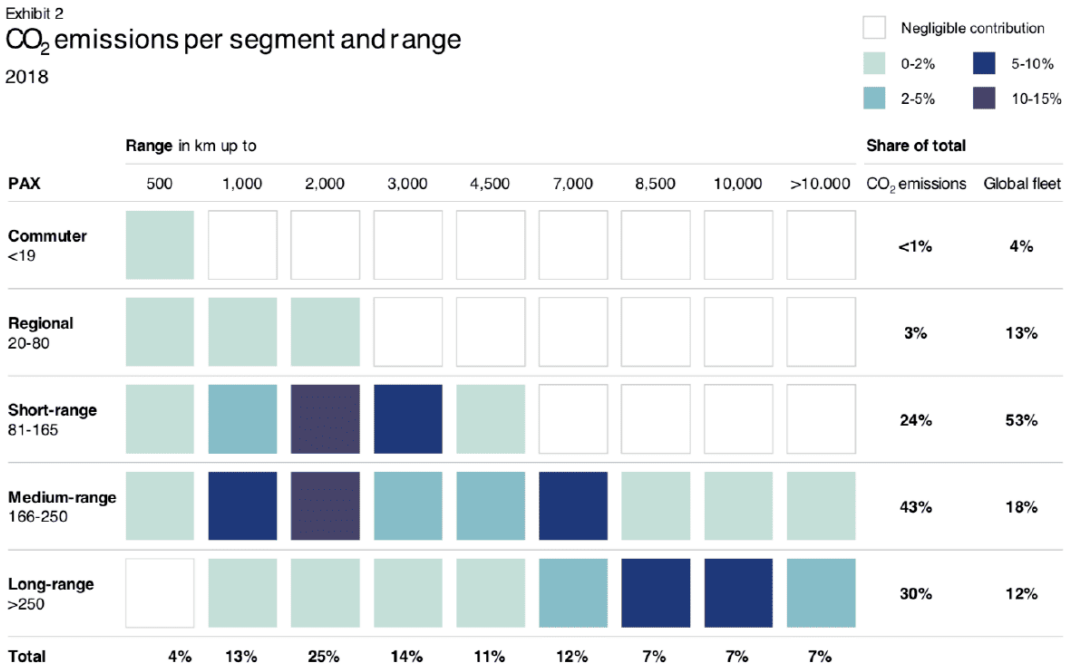

Figure 1.1: CO_2 emission per segment and range [1]

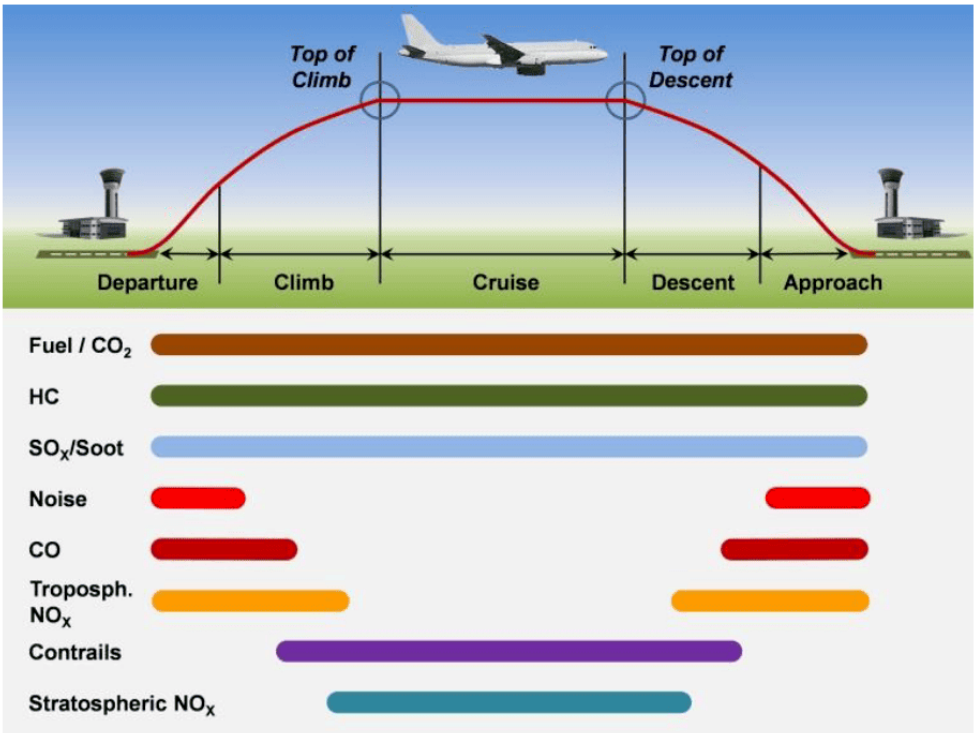

Figure 1.2: In-flight emissions [1]

Similarly, the ICAO table 1.3 distinguishes environmental impacts according to operating altitude, considering distinctly the effects on air quality, fuel consumption, greenhouse gases, and noise based on altitude: at low altitudes, noise and local pollutants dominate; at intermediate altitudes, the effects related to fuel consumption and greenhouse gas emissions are most significant; while at cruising altitude, photochemical and radiative effects become relevant.

Height AGL / Impact	Below 1 000 ft (300 m)	1 000-3 000 ft (300-900 m)	3 000-10 000 ft (900-3 000 m)	Above 10 000 ft (3 000 m)
Air quality (e.g. NOx, PM, etc.)	Most relevant	Relevant (Note 1)	Less relevant	Less relevant
Noise	Potentially (Note 2)	Relevant	Relevant	Potentially (Note 3)
Fuel use / CO_2	Relevant	Relevant	Most relevant (Note 4)	Most relevant (Note 4)
Climate change	Relevant	Relevant	Most relevant (Note 5)	Most relevant (Note 5)

Figure 1.3: Environmental impacts of aviation - table [1]

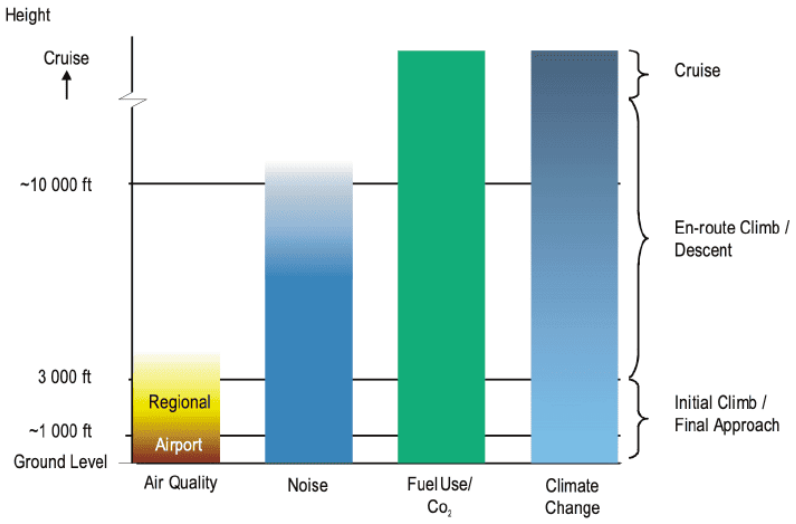

Figure 1.4: Environmental impacts of aviation - graph [1]

A significant environmental impact is also caused by noise, which depends on a number of factors including: the type of aircraft, the number and distribution of daily operations, the time of day, the runways used, the routes flown, weather and topographical conditions, the location and size of surrounding urban areas, the operating procedures adopted, and general operating conditions.

The evaluation of these impacts is usually based on mathematical models with standard databases suggested by the ICAO, such as Aircraft Noise and Performance (ANP) for noise and the ICAO Engine Emissions DataBank for emissions, which, however, assume

normal operating conditions and therefore can't consider actual changes in operations. Parameters like mass, thrust, and wing configuration change a lot based on operating and environmental conditions, making these models not as useful for doing specific analyses for each flight.
The most accurate data comes from flight data recorders (FDRs), but these are privately owned and difficult to obtain for research purposes, or from other sources, such as ADS-B datasets or radar data, but these lack key details such as mass, thrust and flap settings. For this reason, these values often have to be estimated, and several studies have worked on this, including that of Cremaschi and Askari [2], used in this thesis thanks to the collaboration with ENV-ISA.

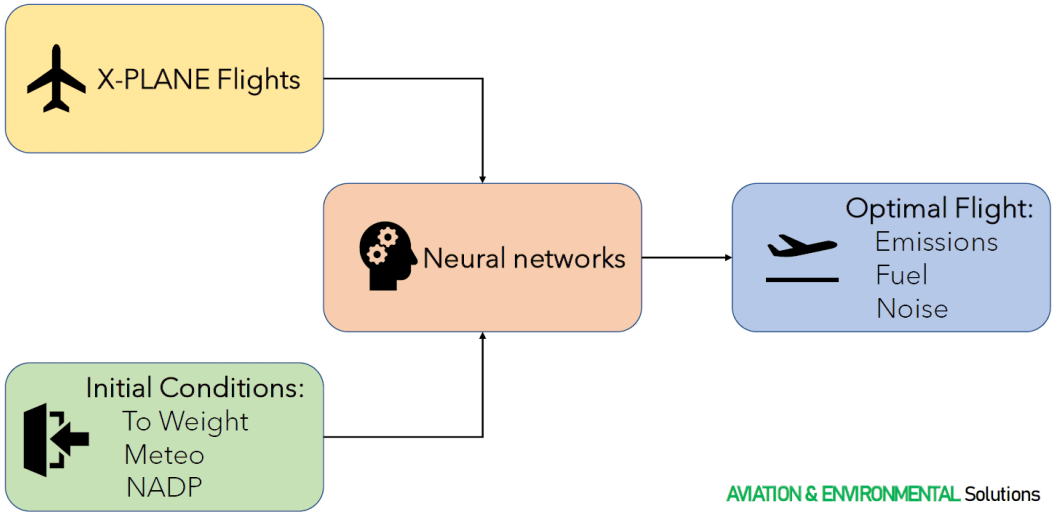

Figure 1.5: Derive optimal profile to minimize a certain objective (©ENV-ISA)

1.2 METHODOLOGY

The methodology adopted [2] is based on the combined use of simulations to generate realistic flight data and the application of predictive models to estimate operational parameters that cannot be directly observed.

The X-Plane simulator was used, chosen for its accuracy in calculating aerodynamic forces using blade element theory, which guarantees a realistic representation of subsonic and transonic flight conditions.

To generate the data needed for the analysis, autopilot algorithms were implemented in Python and connected to the simulator via the X-Plane Connect API in order to automate the generation of a large amount of trajectories with variations in weight, weather conditions, and flap configurations, ensuring data diversity and model generalization capabilities. The collected data was then transformed into formats similar to those of surveillance technologies (ADS-B and radar) and used to train and validate multilayer perceptron neural network models, designed to estimate key parameters such as mass,

thrust profile, and flap configuration, using only variables accessible from surveillance data.

This approach overcomes the limited availability of proprietary data (e.g., Flight Data Recorder) and provides a solid basis for more accurate environmental assessments, such as optimizing flight operations to reduce environmental impact in the LTO cycle, as illustrated in Figure 1.6.

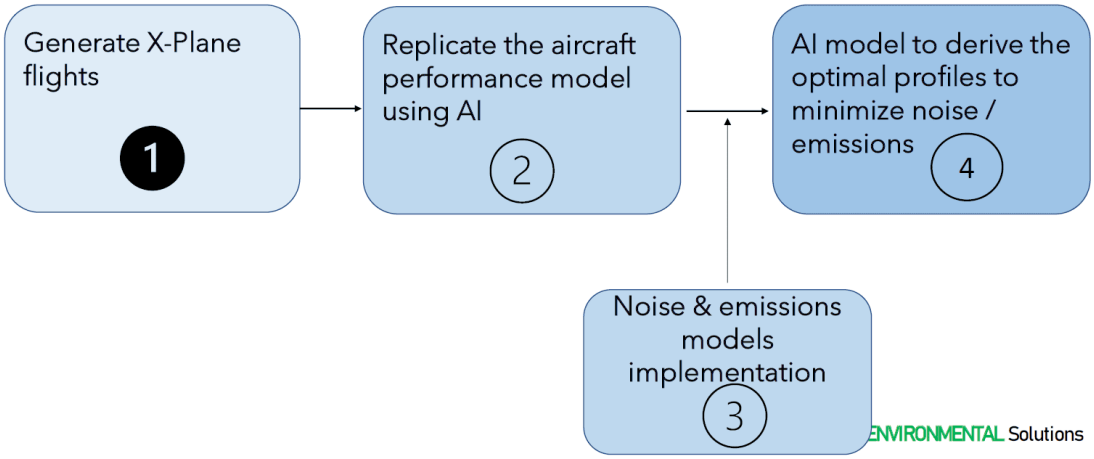

Figure 1.6: Optimization process - workload (©ENV-ISA)

In the final step of the process shown, optimization uses the predictive models trained earlier to quickly generate a large number of plausible operating profiles and integrates the environmental models needed to assess the impact of the flight profiles generated. In particular, the noise model according to **ECAC Doc 29** and the **BFFM2 model** for estimating gaseous pollutants are used, while a model dedicated to particulate matter is still being developed.

The goal is to identify the combination of flight parameters that minimizes noise and/or emissions impact while ensuring compliance with regulatory constraints.

1.3 CASE STUDY

The information provided in Section 1.1 regarding emissions during LTO phases applies to subsonic aircraft, while for high-speed aircraft (supersonic or hypersonic), two additional environmental impacts are considered particularly relevant [1]:

- **Ozone depletion:** supersonic aircraft typically operate at much higher altitudes than subsonic aircraft (approximately 18–20 km for Mach 5 and 30–35 km for Mach 8), coming into contact with the stratosphere, with possible effects on the ozone layer and the atmospheric radiation balance.
- **Sonic boom:** supersonic flight generates shock waves that propagate to the ground as a loud noise, known as a sonic boom, which can have negative effects

on local communities, including possible damage to buildings. For this reason, regular supersonic flights over land are prohibited in many countries.

Historically, the use of civil supersonic flights has remained limited due to high fuel consumption and the resulting ticket costs, in addition to the significant environmental and noise impact of the aircraft, which made it difficult for local communities to accept them [3].
However, in recent years, growing demand for reduced travel times and the availability of more efficient and sustainable propulsion technologies has reignited interest in this category of aircraft.

In this context, the case study of this thesis concerns a Mach 2 aircraft, called **CS1a** [Fig. 1.7], designed as part of the MOREandLESS project.

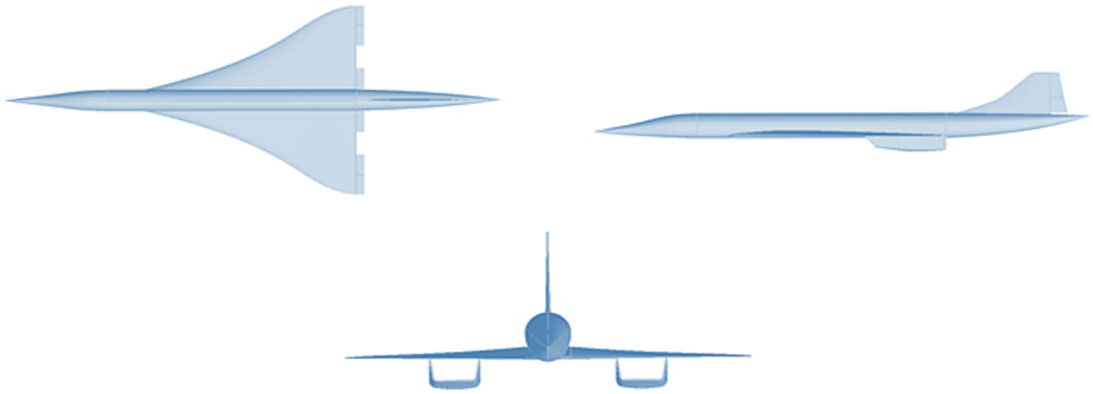

Figure 1.7: Three CS1a vehicle perspectives

The name stands for **MOREandLESS - MDO and REgulations for Low-boom and Environmentally Sustainable Supersonic aviation** and is an international research project funded by the European Union under the Horizon 2020 program. [Fig. 1.8] The main objective of the project is to develop a safe and environmentally friendly supersonic civil aviation system by dealing with two key challenges of supersonic aviation: reducing sonic boom and mitigating the overall environmental impact. The initiative is not limited to technological research, but also extends to collaboration with European Union and US regulatory bodies to define new standards and regulations for supersonic civil aviation at an international level. [4]

Figure 1.8: MOREandLESS project [4]

1.4 THESIS STRUCTURE

The work is structured into five distinct chapters:

- **Chapter 2 – State of the art:** describes the regulatory framework and models used to assess noise and emissions, with reference to supersonic aircraft.
- **Chapter 3 – Aircraft modelling:** introduces the CS1A aircraft and its modelling in Plane-Maker.
- **Chapter 4 – Simulations:** presents the generation of simulated flight data and the training of neural networks to estimate unobservable parameters.
- **Chapter 5 – Optimization:** describes the optimization algorithm for flight profiles to minimize noise, emissions, or other objectives.
- **Chapter 6 – Results:** presents the results obtained.

Chapter 2

STATE OF ART

Nowadays, the aviation industry is paying greater attention to environmental sustainability, which is why it is re-evaluating the way it operates and designs aircraft with the aim of reducing both the noise impact and atmospheric emissions associated with flight operations. In particular, the landing and take-off phases, known as the **LTO cycle**, are considered among the most critical in terms of disturbance to nearby communities and the release of pollutants.

This chapter examines the current regulatory framework and models used for assessing noise impact and emissions during the landing and takeoff cycle, together with the main operational procedures for noise reduction. Since supersonic aircraft present specific environmental and regulatory issues, these are discussed in a section at the end of the chapter.

2.1 NOISE REGULATIONS

Regulation of aircraft-generated noise is defined globally by the International Civil Aviation Organization (ICAO) through the **Annex 16 – Volume I: Aircraft Noise** [5].
However, in addition to ICAO standards, there are national regulations and prediction models that complete the regulatory framework: **Doc 29 ECAC** [6–8] in Europe, while in the US the FAA has developed two distinct regulations: the **14 CFR Part 36** [9], which concerns aircraft noise certification, and the **14 CFR Part 150** [10], about the planning and management of airport noise.
They are all examined in the following sections.

2.1.1 ICAO Annex 16 - Volume 1

As noted in the Historical Background section of [5], the regulation originated from the growing concern about the noise impact of air traffic near airports when, in the late 1960s, an increase in the number of flights and the introduction of new aircraft caused a rise in the noise perceived by local communities.
Following suggestions from the Fifth Air Navigation Conference (1967) and the London Noise Conference (1966), the ICAO Assembly asked the Council to create shared

rules for measuring, certifying, and limiting airplane noise and this led to Annex 16 – Aircraft Noise (later added to Annex 16 – Environmental Protection), which today is the main source for Standard and Recommended Practices (SARPs) regarding airplane noise and its environmental effects.

Chapter 14 [5], which was introduced in the 8th edition (Amendment 11-B), sets particular noise limits for subsonic planes, based on their certified takeoff mass and when the type certificate was applied for.:

- Subsonic jet and propeller-driven aircraft $MTOM \geq 55.000$ kg (certification after December 31, 2017)
- Subsonic jet aircraft $MTOM < 55.000$ kg (certification after December 31, 2020)
- Propeller-driven aircraft $MTOM$ tra 8.618 kg e 55.000 kg (certification after December 31, 2020)

Noise is measured using the **Effective Perceived Noise Level (EPNL)**, expressed in EPNdB units, and considers how people perceive aircraft noise, taking into account three key factors: instant sound level, adjustements for spectral irregularities, and adjustment for how long the sound lasts.

The EPNL calculation involves five main steps, as detailed in Appendix 2 of [5]:

1. **Conversion to "perceived noisiness" (noy):**
   The measured acoustic signal is divided into 24 one-third octave bands. For each 0.5 s interval, the sound pressure level (SPL) is computed in band 'i' at time 'k' , then these values are converted into units of perceived noisiness (noy) using tables or math formulas.

2. **Calculation of Perceived Noise Level (PNL):**
   The perceived noise contributions from different bands are summed to get the total noise at time k, which is converted into Perceived Noise Level.

3. **Tonal correction**
   A correction factor, C(k), is applied to consider pure tones or peaks in the spectrum. The result is the Tone-Corrected Perceived Noise Level (PNLT).

   $$PNLT(k) = PNL(k) + C(k)$$

4. **Identification of the maximum level and actual duration:**
   The PNLT(k) temporal profile helps figure out the maximum perceived level and the actual duration of the event, defined as the time interval in which the level remains within 10 dB of the maximum

5. **Calculation of EPNL:**
   PNLT(k) levels are summed over time using a logarithmic scale and normalized to a reference duration of 10 s. The result is the final index EPNL.

The calculation described is done at three reference points representing the most critical conditions for sound perception:

- **Flyover:** along the runway axis, 6.5 km from the takeoff start point.
- **Sideline:** 450 m from the central runway line, where the power reaches its peak.
- **Approach:** on the approach path, about 2 km from the expected touchdown point.

For each point, an EPNL value is calculated and compared to ICAO regulatory limits, as none of the three values should exceed these limits.

2.1.2 ECAC Doc 29

While ICAO sets global standards for noise certification, the European Civil Aviation Conference (ECAC) focuses on noise modeling for airport management and planning in Europe, using Doc 29 as main reference.
The fourth edition of this document is available, divided into three volumes, each with a specific function:

- **Volume 1** serves as a beginner's guide for those working with noise models, such as airport planners, environmental consultants, and policymakers. It plainly explains the basics of modeling, its uses, and its limits, and gives practical advice on understanding the results. It has a section on the aircraft substitution method, which is helpful when the actual aircraft isn't in the international ANP (Aircraft Noise and Performance) database. It also introduces the new Volume 3, which focuses on model verification and validation. [6]
- **Volume 2** is the technical part that defines the official European Civil Aviation Conference (ECAC) method for computing noise contours around airports. It includes the necessary algorithms and procedures for creating consistent models, but does not include the code itself. The goal is to ensure agreement among countries and to have a standard for simulation software. The method is flexible and can adapt to different levels of detail, but it always requires comparison with real measurements to maintain accuracy. [7]

  A key part of Volume 2 involves making **acoustic contour maps**, which are created using noise curves, based on flight paths, operational setups, and aircraft noise data and show how noise spreads around airports.
  These maps are a main source for land planning (for example, they help to spot areas that may not be suitable for residential use), environmental assessment, and future scenario analysis.
- **Volume 3, Part 1** is for model developers, used to check if new tools follow the Volume 2 methods. It gives full example problems, with input data and expected results, to test and approve models. The goal is to ensure consistency across different software in Europe. A future Part 2 will focus on experimental validation, comparing models with actual noise data. [8]

In conclusion, Doc 29 is important because it suggests a standard way to predict noise from air operations and create noise contour maps.

Besides this document, it is important to mention the **Aircraft Noise and Performance database**. [11] EUROCONTROL, with help from ECAC and ICAO, developed this archive that gathers a range of acoustic and performance data for many aircraft, including:

- Noise-Power-Distance (NPD) curves, which allow calculation of noise propagation as a function of engine power and distance;
- Standard operational profiles for different phases of the flight (takeoff, climb, approach).
- Operational settings and specific aircraft info, useful to tell varied models apart.

When an aircraft is not in the database, the substitution method from Volume 1 is used, so an equivalent aircraft is selected based on noise and performance attributes.

By combining Doc 29 methods with ANP data, the noise model results are updated, consistent, and comparable, ensuring an international agreement in predicting and assessing airport noise.

2.1.3 FAA 14 CFR Part 36

In the United States, noise regulation is regulated by the Federal Aviation Administration (FAA), which sets aircraft acoustic certification standards through 14 CFR Part 36 [9], similar to the European approach.
This regulation defines noise measurement procedures during flight phases, sets maximum permissible limits for each aircraft category, and introduces the following certification categories:

- **Stage 1:** aircraft that do not meet Stage 2 limits (now not accepted for new certifications).
- **Stage 2:** it provides less strict limits, applied to aircraft certified before the 1980s.
- **Stage 3:** standard for several years, with stricter limits.
- **Stage 4:** introduced to decrease noise impact.
- **Stage 5:** the newest, most strict version, which became required for new certifications starting December 31, 2017 with $MTOM \geq 55.000$ kg and from December 31, 2020, for lighter aircraft.

The requirements become stricter as noise reduction improves: Stage 1 is quite loud, while Stage 5 is the quietest.

The Effective Perceived Noise Level (EPNL), measured in EPNdB, is still the metric for rating noise, and its calculation follows procedures close to those of the ICAO (2.1.1). A main difference is that the FAA sets its numerical limits (Appendix B of [9]), while the measurement points stay the same in relative position but with specific operational details:

- **Lateral full-power:** 450 m from the central runway line, at the point of maximum power.
- **Flyover:** 6.500 m from the start of the take-off run.
- **Approach:** 2.000 m from the runway threshold, 120 m below the approach trajectory at 3°.

2.1.4 FAA 14 CFR Part 150

In addition to Part 36, 14 CFR Part 150 [10] regulates airport noise planning and management to assess the compatibility between airport operations and the use of surrounding land.
The document's introduction outlines its scope and purpose, specifically:

- to measure noise levels at airports and in nearby areas;
- to determine individual exposure to noise from airport operations;
- to identify land uses that are compatible with different levels of noise exposure.

When comparing FAA 14 CFR Part 150 with ECAC Doc 29, similar methods are used. Both documents include creating noise contour maps based on noise propagation models and airport data. These maps are a useful tool to support land-use planning and environmental assessment.
The difference is that Doc 29 focuses on technical standardization of models and consistency between software used across different countries. Part 150 , on the other hand, gives more importance to public involvement, consultation with local authorities, and the chance for endorsement by the aviation authority.

2.2 AIR EMISSION REGULATIONS AND MODELS

The environmental impact of aviation is not only about noise, but also about atmospheric emissions produced by the combustion of fuel in aircraft engines.
The effects of these emissions are visible:

- Locally, as they affect air quality near airports through the production of primary pollutants such as nitrogen oxides (NO_x), carbon monoxide (CO), unburned hydrocarbons (HC) and particulate matter.
- Globally, as they alter the chemical and radiative composition of the atmosphere through the emission of carbon dioxide (CO_2), water vapour (H_2O) and soot particles, affecting the climate and the greenhouse effect.

Emissions are quantified based on the fuel burned, using indices that correlate engine operating conditions with the amount of pollutants released.

This chapter analyses [1]:

- the main international regulations governing the certification of aircraft engine emissions;
- the description of the LTO (Landing and Take-Off) cycle, used as a reference for measuring and classifying emissions;
- prediction models, in particular the Boeing Fuel Flow Method 2 (BFFM2), widely used to estimate emissions during flight.

2.2.1 ICAO Annex 16 - Volume 2

International regulations related to aircraft engine emissions are specified in ICAO Annex 16 – Volume II: Aircraft Engine Emissions. [12] which defines the procedures for certifying engines, in order to limit emissions of nitrogen oxides (NO_x), carbon monoxide (CO), unburned hydrocarbons (HC) and visible smoke, quantified using the Smoke Number (SN).

One of the main objectives of the ICAO is to reduce the impact of emissions on **local air quality**, especially in areas near airports, and to do that Volume II establishes Standards and Recommended Practices (SARPs), meaning:

- Standard: mandatory for Member States.
- Recommended Practice: non-obligatory recommendations, but considered important for improving safety and efficiency.

The certification is based on the LTO (Landing and Take-Off) cycle, which represents typical operations during take-off and approach phases, but will be described in detail in the next section.
The test results are collected in the **ICAO Engine Emissions Databank** [13], managed by ICAO and EASA. This database contains data on emissions from engines in production and is used for environmental analysis and to validate predictive models, such as the Boeing Fuel Flow Method 2 (BFFM2).

The review and updating of ICAO standards is managed by the Committee on Aviation Environmental Protection (CAEP), which has introduced important changes over the years:

- Standard for non-volatile particulate matter (nvPM) based on visibility criteria (CAEP/10).

[1] Reference for these topics: slides from the course "Gestione dei rischi, costi e supporto logistico integrato dei sistemi aerospaziali", academic year 2023/2024, Politecnico di Torino, lectures by Professors N. Viola and R. Fusaro.

- Standard for nvPM particle mass and number, adopted in 2020 and in force since 2021 (CAEP/11).

- New, more stringent rules for NO_x emissions in the LTO cycle, currently being developed for 2025-2028.

Besides gas emissions and particulate matter, the ICAO provisions also consider liquid fuel discharge, providing a complete approach for the environmental certification of jet engines.

2.2.2 Emissions during the LTO cycle

This section shows a model for calculating the amount and type of emissions from civil subsonic aircraft engines [1,14], while supersonic aircraft will be discussed in detail later.

The Landing and Take-Off (LTO) Cycle, defined by the ICAO, represents the typical behaviour of an engine during near-ground phases and is used by engine manufacturers as a reference for performing emission tests before certifying a new model.

The cycle consists of four operating modes, each one characterised by a specific thrust level and a standard duration:[Tab 2.1, Fig 2.1]

- **Take-off:** phase in which the engine operates at maximum power to allow the aircraft to take off.

- **Climb-out:** phase following take-off, during which the engine provides the thrust necessary for climbing to transition altitude.

- **Approach:** phase in which the aircraft prepares for landing and engine thrust decreases.

- **Idle:** phase in which the engine operates at minimum speed, typically during taxiing or waiting on the ground.

Operating Mode	**Thrust setting [%]**	**Time in operating mode [min]**
Take-off	100	0.7
Climb	85	2.2
Approach	30	4.0
Taxi/ground idle	7	26.0

Table 2.1: ICAO requirements for the LTO cycle - subsonic [12].

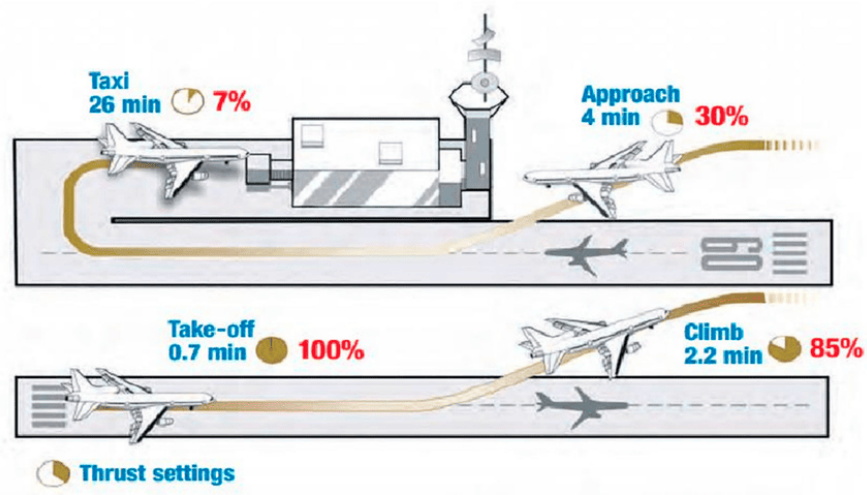

Figure 2.1: Stages of the LTO cycle

During fuel combustion, various chemical and radioactive substances are produced and discharged into the atmosphere as solid and gaseous emissions and their **Emission indices (EI)** are defined as the amount of pollutant (in grams) produced per kilogram of fuel consumed.
The main gaseous emissions include CO_2, H_2O, SO_x, NO_x, CO and unburned hydrocarbons (HC) and can be divided into two main categories:

- **Emissions directly linked to the amount of fuel burned**: these include CO_2, H_2O and SO_x, for which a constant emission index is assumed:

$$EI_{CO_2} = 3160 \text{ g/kg}, \quad EI_{H_2O} = 1240 \text{ g/kg}, \quad EI_{SO_x} = 0.6 \text{ g/kg}$$

- **Emissions depending on the combustion process**: these include NO_x, CO and HC.

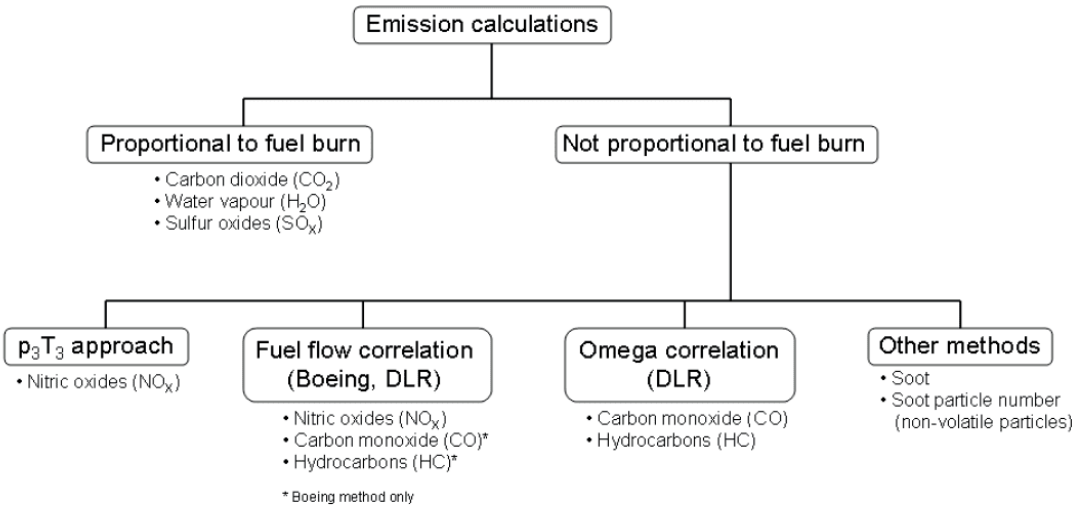

Figure 2.2: Overview of methods for calculating emissions [14]

As shown in Figure 2.2, emission calculations for NO_x, CO, and HC require more complex models compared to species proportional to fuel consumption.
To simplify the estimation of this type of emissions during flight, **fuel flow correlation methods** have been developed. These semi-empirical approaches are based on the assumption that in-flight emission indices can be compared to reference values at sea level (EI_{ref}) and vice versa, and they allow to estimate emission indices (EI) based on engine fuel flow ($\dot{w}_{fuel}$), atmospheric conditions and flight speed, following these three main steps [Fig2.3]:

1. Reducing the in-flight fuel flow ($\dot{w}_{fuel}$) to the reference conditions at sea level ($\dot{w}_{fuel,ref}$).

2. Determining the reference emission index (EI_{ref}) as a function of $\dot{w}_{fuel,ref}$, using EI–fuel flow curves derived from ICAO data.

3. Converting the reference emission index (EI_{ref}) to actual flight conditions (EI).

The following paragraph will focus on a detailed explanation of the **Boeing Fuel Flow Method 2 (BFFM2)**.

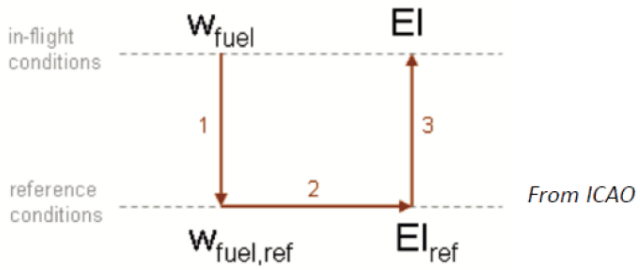

Figure 2.3: Fuel Flow Methods

Once all emission indices are known, the total amount of emissions can be calculated. For each phase of the mission and for each combustion product, the following formula is used:

$$\text{Emission}_{i,k} = EI_{i,k} \cdot \dot{w}_{f,k} \cdot \Delta t$$

where: i denotes the emission type, k denotes the phase of the LTO cycle, $\dot{w}_{f,k}$ is the fuel flow in phase k, Δt is the time duration of the phase.

2.2.3 Boeing Fuel Flow Method 2

The Boeing Fuel Flow Method 2 (BFFM2) is used to calculate NO_x emission indices, but also to estimate CO and HC indices for specific flight conditions. The process consists of three main steps:

1. As in the method developed by DLR, the first step is to derive the reference fuel flow, $\dot{w}_{fuel,ref}$, from the in-flight fuel flow, $\dot{w}_{fuel}$.

2. Next, the relationship between emission indices (EI) and fuel flow is obtained using data from the ICAO database.
   Unlike the DLR method, Boeing introduces a correction factor r that takes into account the effects of engine installation on the aircraft. This correction is applied to the fuel flow values from the ICAO database, obtaining a corrected curve from which, in correspondence with $\dot{w}_{fuel,ref}$, the emission indices at reference conditions EI_{ref} are obtained.

3. Finally, the reference emission indices EI_{ref} obtained in the previous step are re-corrected to actual flight conditions using the equations highlighted in the flow chart in Figure 2.7, thus obtaining the final emission indices EI,

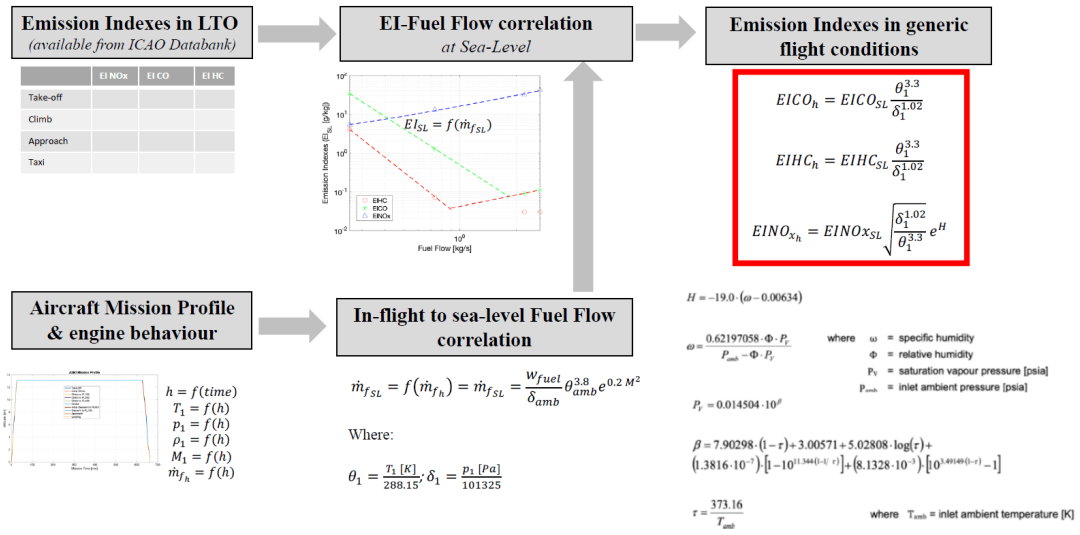

Figure 2.4: Boeing Fuel Flow Method 2 - subsonic [1]

2.2.4 Non-volatile particulate matter (nvPM) emissions

In addition to gaseous emissions, aircraft engines produce **non-volatile particulate matter (nvPM)**: which mainly consists of solid carbon particles (soot) generated during fuel combustion, affecting both local air quality and the global climate. [15]
It is exactly because of the growing scientific evidence of their negative effects on environment and health that regulations have only recently begun to consider this type of emissions.
The international regulations on nvPM emissions are defined in ICAO Annex 16 - Volume II [12], with updates introduced on the recommendation of the CAEP (Committee on Aviation Environmental Protection), particularly in meetings **CAEP/10** and **CAEP/11**.

Emissions are defined in terms of the Emission Index (EI):

- EI_{mass}, expressed as grams of nvPM per kilogram of fuel;

- EI_{number}, indicating the number of particles per kilogram of fuel.

Since January 1, 2023, all engines exceeding 26.7 kN of thrust must observe specific limits for both parameters, measured during the LTO (Landing and Take-Off) cycle and reported under standardised conditions.
The results of certification tests are collected in the ICAO Engine Emissions Databank (EEDB), managed by EASA. [13]

When certified experimental data are not available, or for engines not subject to direct regulation, we can use empirical estimation methods based on more easily measurable parameters, such as the **Smoke Number (SN)**.
The most widely used method as reference for air quality modelling in airports is **First Order Approximation version 4 (FOA4)**, described in ICAO Doc 9889 – Airport Air Quality Manual [16] and summarised in the following steps:

1. **Conversion of Smoke Number (SN):**
   SN is converted to a mass concentration of non-volatile particulate matter (C) using an empirical correlation based on experimental data obtained under conditions similar to those of certification.

2. **Calculation of exhaust gas volume:**
   Based on the air-fuel ratio (AFR) and, if necessary, the bypass ratio (BPR) of the engine, we estimate the volume of exhaust gases produced per kilogram of fuel (Q).

3. **Determination of the mass emission index ($EI_{nvPM,mass}$):**
   The product $C \cdot Q$ gives the mass emission index of non-volatile particulates, expressed in grams per kilogram of fuel.
   Since particulate measurements can be affected by physical losses in the sampling system, FOA4 includes an empirical correction to compensate for these losses and obtain representative values at the engine outlet.

4. **Estimation of the number emission index ($EI_{nvPM,number}$):**
   The number emission index is estimated starting from the corrected value of $EI_{nvPM,mass}$, using additional parameters such as the geometric mean particle size, density and other physical properties of the particulate matter.

In order to extend emissions measurement to include flight phases and not just near-ground phases, the ICAO is developing a methodology based on interpolation of LTO cycle data and correction for operating conditions at altitude.
This approach is still under experimental validation and has more uncertainties than well known methods for other pollutants, like the Boeing Fuel Flow Method 2 (BFFM2) for nitrogen oxides (NO_X). The main challenges are due to the variability of nvPM emission curves and the limited availability of experimental data during cruise. [15]

2.3 NOISE ABATEMENT DEPARTURE PROCEDURES (NADPs)

ICAO recommendations on airport noise reduction can be found in **Doc 8168, Volume I – Flight Procedures** [17] and Part I, in particular, contains guidelines on preferred runways and routes for noise reduction, displaced thresholds, approach and landing procedures, and Noise Abatement Departure Procedures (NADP).
These procedures are part of the **ICAO's Balanced Approach** to noise management, based on identifying the noise problem at each airport and analysing the possible measures to reduce its impact, which are:

- noise reduction at source via technological standards,
- land use planning and management,
- noise reduction operating procedures, such as **NADPs**
- operating restrictions on aircraft.

ICAO supports the development and standardisation of low-noise procedures that are safe and economically viable, and states that "Nothing in these procedures shall prevent the pilot-in-command from exercising authority for the safe operation of the aeroplane". [17].
From the operational point of view, NADPs work on the coordinated control of thrust, aerodynamic configuration (flaps/slats) and speed during the initial climb, and we can choose between two main types: NADP1 and NADP2. This choice depends on local factors like the orientation of the runways, the layout of the take-off routes and the local community's needs.

This chapter analyses the two types of NADP and their environmental impacts in terms of noise and emissions.

2.3.1 Types of NADPs

Noise Abatement Departure Procedures (NADP) are intended to reduce the perceived ground noise during take-off and initial climb and, in particular, it's possible to distinguish between two types of NADP, each one optimised to mitigate the acoustic impact in different areas around the airport.
The specific description of these procedures is contained in the appendix to Chapter 3 of [17]:

- **NADP 1** focuses on reducing noise in the immediate vicinity of the runway, especially for communities located under the take-off path. The procedure provides for:
  - thrust decrease starting at a minimum altitude of 240 m (800 ft) above the airport elevation;
  - delay in flap/slat retraction, which only occurs when the maximum prescribed altitude of 900 m (3,000 ft) is reached;

– steeper initial climb, which concentrates noise reduction in areas close to the runway.

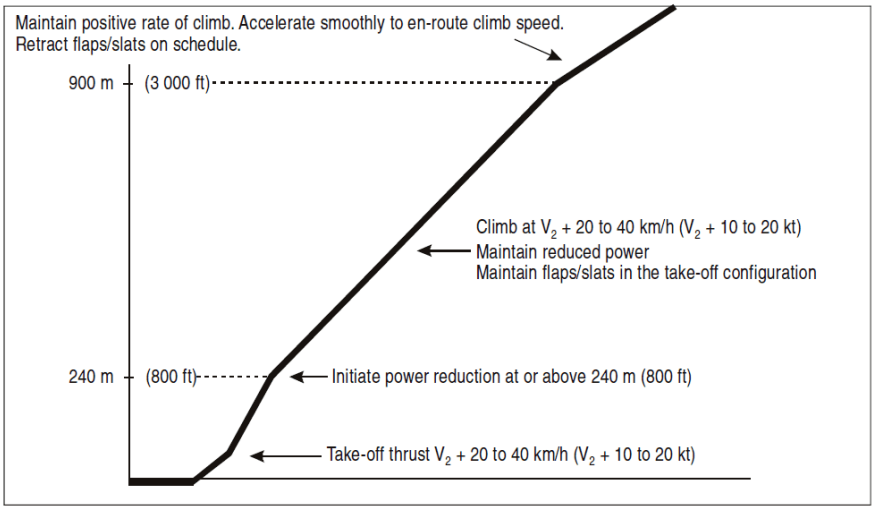

Figure 2.5: Example of NADP1 [17]

- The **NADP 2**, on the other hand, focuses on reducing noise in areas further away from the airport. The procedure provides for:
  - retraction of flaps/slats as soon as the minimum altitude of 240 m is reached, with thrust reduction occurring either simultaneously or immediately afterwards;
  - early acceleration, which allows a faster transition to clean configuration and a more efficient climb speed;
  - a less steep initial climb profile, shifting noise reduction to higher altitudes.

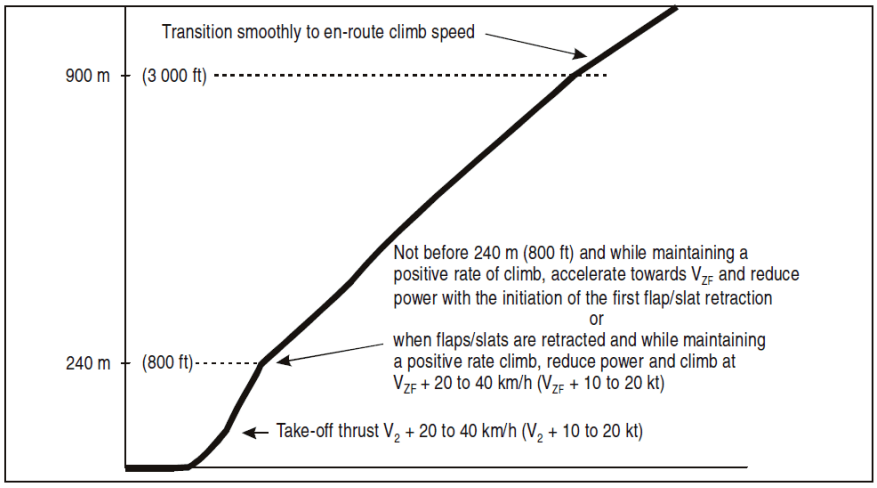

Figure 2.6: Example of NADP2 [17]

In both procedures, power reduction may not begin before the minimum prescribed altitude, the initial climb speed before acceleration must be maintained between V_2 + 20–40km/h (10–20kt), and once 900 m (3,000 ft) is reached, the transition to en-route climb speed occurs.

The choice of the NADP procedures depends on the operational and environmental characteristics of each airport, in fact, aerodrome operators determine which is most suitable based on the location of populated areas and noise reduction objectives. In general, NADP 1 is preferable when sensitive areas are located very close to the runway and noise needs to be reduced in the initial stages of take-off, while NADP 2 is more suitable when populated areas are located further away from the airport, permitting a more efficient take-off profile.
After verifying that the procedures comply with ICAO Doc 8168 guidelines, the state of the operator may proceed with the approval and the procedures are published in the national AIPs and integrated into the airlines' operating manuals. However, in the Operational Limitations section [17], it is specified that "the pilot-in-command has the authority to decide not to execute a noise abatement departure procedure if conditions preclude the safe execution of the procedure", which is because flight safety must always take priority over noise reduction.

2.3.2 Effects of NADPs on noise and gaseous emissions

The PANS-OPS guidelines [17] focus primarily on safety and noise reduction, without considering that NADP procedures also significantly affect engine emissions during initial climb. For this reason, ICAO conducted a study, published in **Circular 317-AT/136** [18], on the gas emissions of these procedures to demonstrate that NADP 1 and NADP 2 differ not only in terms of the area in which they ensure noise reduction, but also in terms of their effects on fuel consumption and the formation of gaseous pollutants.
The study considered different types of aircraft and simulated four variants of procedures (two NADP 1, named procedures 1 and 2, and two NADP 2, named procedures 3 and 4) to estimate how noise levels and emissions change as a function of the cutback altitude, i.e. the height at which power reduction occurs, and the acceleration phase.

As already mentioned in the previous paragraph, this study also confirmed that NADP 1 is more effective in reducing noise in areas close to the runway ("close-in area"), due to the earlier thrust reduction and steeper climb, while NADP 2 shifts the acoustic advantages to more distant areas ("distant area"), reducing the noise impact several kilometres away from the airport. The differences are most noticeable in the close-in area, where they can reach up to 8 dBA.
However, from an environmental point of view, NO_x and CO_2 emissions show opposite behaviour: a procedure characterised by a smoother climb reduces overall fuel consumption, thereby reducing carbon dioxide emissions, but involves higher combustion temperatures, thus increasing nitrogen oxide emissions. For this reason, the results show that NADP 2 tends to produce less CO_2 (reductions between 0.6% and 2.7%) but more NO_x (increases of up to 20% for wide-body aircraft) than NADP 1.

So there is not a single procedure that optimises both noise and emissions, but the choice must be evaluated case by case: NADP 1 is recommended for airports surrounded by densely populated areas near the runway, while NADP 2 is more suitable where noise-sensitive areas are more distant or when fuel consumption needs to be optimised.

2.4 REGULATION AND STUDIES ON SUPERSONIC AIRCRAFT

Up to now, we have discussed the regulations and models related to subsonic aircraft, so that we can now discuss supersonic aircraft in a specific section, as the aircraft object of this thesis belongs to this category.
Unlike subsonic aircraft, supersonic aircraft present particular challenges related to noise, especially sonic booms and acoustic emissions during take-off and landing, and atmospheric emissions.
The articles by Rotger et al. [3] and Piccirillo et al. [19] were fundamental in exploring the topics covered in this section.

2.4.1 Noise regulations and models

Within the ICAO noise regulations, i.e. **Annex 16 Vol. 1** [5], Chapter 12 specifically deals with supersonic aircraft. However, it doesn't set numerical noise limits, as it does for subsonic aircraft, but simply states that the same type of aircraft shouldn't exceed the noise levels of the first certified model, which was the Concorde in 1976.

In the United States, meanwhile, the reference is **FAA 14 CFR 36** [9], but even in this case, the rules for supersonic aircraft are limited to prohibiting supersonic flight over the continental United States, except for specific authorisations for testing or research.
Both regulations are therefore very outdated, because after Concorde ceased service in 2003, no more civil supersonic aircraft were certified, and consequently the ICAO or FAA regulatory standards were not updated. To fill these gaps and provide more appropriate guidelines for next-generation SST certification, ICAO has started a review and update process through the Committee on Aviation Environmental Protection (CAEP), and its activities are divided into three main cycles:

- **CAEP/11 (2016–2019)**: ICAO focused its work on defining the method for measuring sonic booms, i.e. the noise generated during supersonic flight. The main objectives were:
  - to identify ground measurement points for assessing sonic boom noise;
  - to select an appropriate acoustic metric to correlate human perception indoors and outdoor measurements;
  - to assess the benefits of using predictive models of sonic booms, in addition to actual physical measurements.

- **CAEP/12 (2019–2022)**: conducted an exploratory study on the environmental performance of future supersonic aircraft. The analysis covered:
  - LTO (Landing and Take-Off) noise
  - NO_x emissions during LTO, which affect air quality at airports;
  - cruise emissions (cruise NO_x), which are relevant to climate impact;
  - fuel consumption
- **CAEP/13 (2022–2025):** the objective is to develop a comprehensive regulatory framework for the certification of future SSTs, with two working groups:
  - WG1 (Noise), focuses on developing a standard for LTO noise from supersonic aircraft and also monitors research on sonic booms and en-route noise;
  - WG3 (Emissions): works on LTO emissions standards and the evaluation of a possible CO_2 standard for SSTs.

In addition to updating regulations, several scientific studies have discussed the need to assess the noise generated by supersonic aircraft early on in the design phase, since the Concorde demonstrated that airport noise generated during take-off and landing, due to greater thrust, speed and lift-off angles, was a very critical issue.
In particular, the study by Piccirillo et al. [19] proposes a simplified methodology for estimating the LTO noise of supersonic aircraft from the early stages of SST development, with a "design-to-noise" approach, which can be summarised in four main phases:

1. Definition of the LTO flight profile
2. Modelling of noise sources (engine, fan, jet, landing gear, flaps, leading and trailing edges) using semi-empirical equations
3. Calculation of acoustic losses in the atmosphere, to correctly estimate the sound level perceived on the ground by observers at the three ICAO measurement points, already seen in the subsonic noise assessment procedure: flyover, sideline and approach.
4. Conversion into certified acoustic metrics

The method was verified on the Concorde, the only civil supersonic aircraft with certified data available in Eurocontrol's ANP (Aircraft Noise and Performance) database, and the results turned out to be reliable, giving useful guidelines for adding LTO noise assessment early on in the design phase to help develop future sustainable SSTs.

2.4.2 Air emission regulations and models

Even in terms of emissions regulations, contained in **ICAO Annex 16 Vol. II** [12], those for supersonic aircraft are based on criteria developed for the Concorde and are consequently outdated and do not reflect the requirements of modern SST designs.
Chapter 3 states: "The provisions of this chapter shall apply to all turbojet and turbofan

engines intended for propulsion at supersonic speeds whose date of manufacture is on or after 18 February 1982", so the limits reported for NO_x, CO, HC and smoke, as well as the test methods, have not been updated, while the new requirements for non-volatile particles (nvPM), introduced in 2017 for subsonic engines, have not been taken into account for supersonic engines. Consequently, current requirements do not consider some of the environmental issues associated with this type of aircraft, such as:

- during LTO, the main emissions include NO_x, CO, HC and particulate matter, with values generally higher than those of subsonic aircraft;
- in cruise, NO_x and water vapour emissions affect ozone chemistry and the radiation balance;
- CO_2, which is directly proportional to fuel consumption, is the main climate emission;
- although contrails may be less frequent than in subsonic flights, water vapour emitted at supersonic altitudes can have a greater impact on the climate than at conventional altitudes.

For this reason, CAEP is considering updating standards, evaluating the alignment of supersonic LTO limits with those of subsonic aircraft and introducing metrics for cruise emissions. [3]

Other differences between subsonic and supersonic aircraft concern the LTO cycle and the Boeing Fuel Flow Method 2 (BFFM2).

Chapter 3 defines a specific LTO cycle for supersonic aircraft, consisting of five operating modes (taxi, take-off, climb, descent and approach) which differ from subsonic cycles in terms of the timing of each phase and thrust levels in order to adapt to the flight characteristics of supersonic aircraft and the use of afterburners, typical of Concorde engines. [Tab 2.2]

Operating Mode	**Thrust setting [%]**	**Time in operating mode [min]**
Take-off	100	1.2
Climb	65	2.0
Descent	15	1.2
Approach	34	2.3
Taxi/ground idle	5.8	26.0

Table 2.2: ICAO requirements for the LTO cycle - supersonic [12].

As concerns the model used to estimate emission indices, the original Boeing Fuel Flow Method 2 (BFFM2) has significant limitations for supersonic aircraft since it doesn't consider the integration between the engine and the airframe, and assumes that the compression between the freestream and the combustor inlet is isentropic, which is not valid in the presence of multiple shocks and supersonic geometries.
To model the process correctly, the BFFM2 is modified by introducing:

- a pressure correction factor (kp), variable with the Mach number, which considers the pressure increase due to multiple impacts;
- a temperature correction factor (kt) to consider thermal effects;
- the division of compression into two stages: a non-isentropic section between the freestream and compressor inlet and an isentropic section between the compressor and combustor.

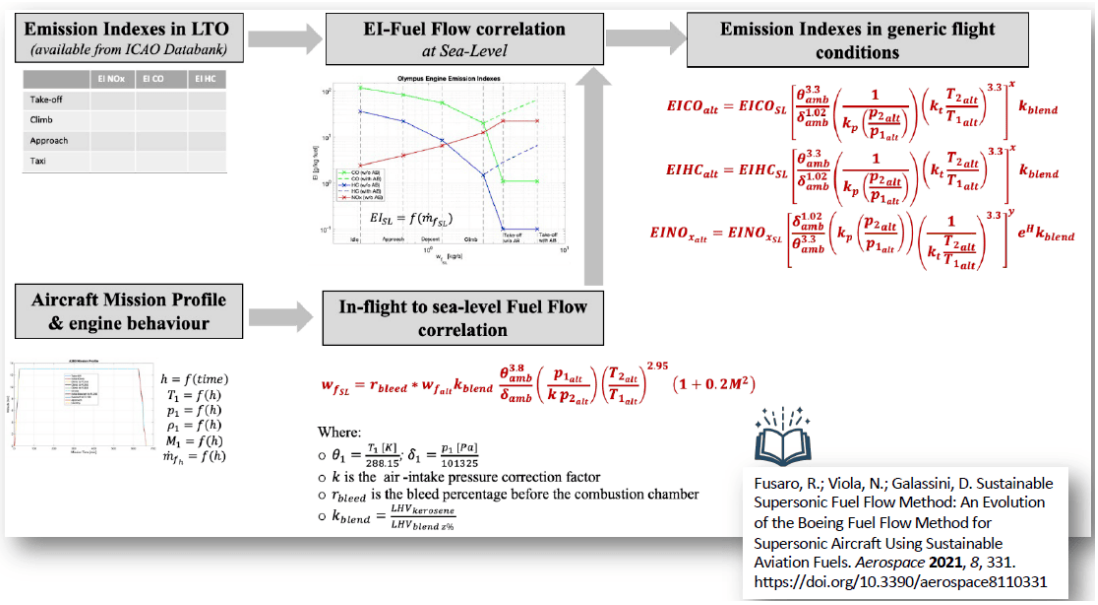

Figure 2.7: Boeing Fuel Flow Method 2 - supersonic [1]

The result of these adjustments is the method shown in the flow chart in the figure and, even though it's still a simplified procedure, it gives realistic estimates of emission indices throughout the mission, which are useful for preliminary assessments during the design phase and for developing sustainable SSTs.

Chapter 3

AIRCRAFT MODELLING

The aircraft analysed in this thesis is the **CS1A**, developed as part of the European **MORE&LESS** project, which focuses on defining sustainable supersonic configurations with low environmental impact, and its configuration is the result of a project developed at the Politecnico di Torino as part of the Integrated Aerospace Systems Design course, which involved the design of a passenger aircraft with a cruising speed of Mach 2. [20]
Like the Concorde, which strongly inspired it, it incorporates the typical characteristics of supersonic aircraft, which are fundamental for reducing drag at high speeds: an extremely slender fuselage, delta wing with integrated elevons and the absence of horizontal tailplanes.
In terms of dimensions, the CS1A has proportions similar to those of the Concorde, and the model was developed in Plane-Maker, which is necessary to create the aircraft to be used in X-Plane simulations.

This chapter first describes the reference aircraft, the Concorde, then the CS1A, and finally explains the modelling process in Plane-Maker.

3.1 CONCORDE

The Concorde was a supersonic passenger aircraft developed by **Aérospatiale** (France) and **British Aircraft Corporation** (United Kingdom), which entered commercial service in 1976 and was retired in 2003, mainly due to three factors: [21]

- the decline in passenger numbers following the accident in 2000;
- the reduction in global demand for scheduled flights after the terrorist events of September 11, 2001;
- the increase in already high maintenance costs.

It was the first (and, actually, the only one in regular Western service) airliner capable of long-range supersonic cruising, flying at about Mach 2.02–2.04 at altitudes close to 18 km (60.000 ft), and allowing transatlantic routes to be covered in reduced times, such as London–New York in about 3.5 hours.

To achieve a non-stop flight across the Atlantic Ocean, Wikipedia states that "Concorde required the greatest supersonic range of any aircraft. This was achieved by a combination of powerplants which were efficient at twice the speed of sound, a slender fuselage with high fineness ratio, and a complex wing shape for a high lift-to-drag ratio" [21].

The following subsections describe in detail the main structural and functional components of the aircraft. [21, 22]

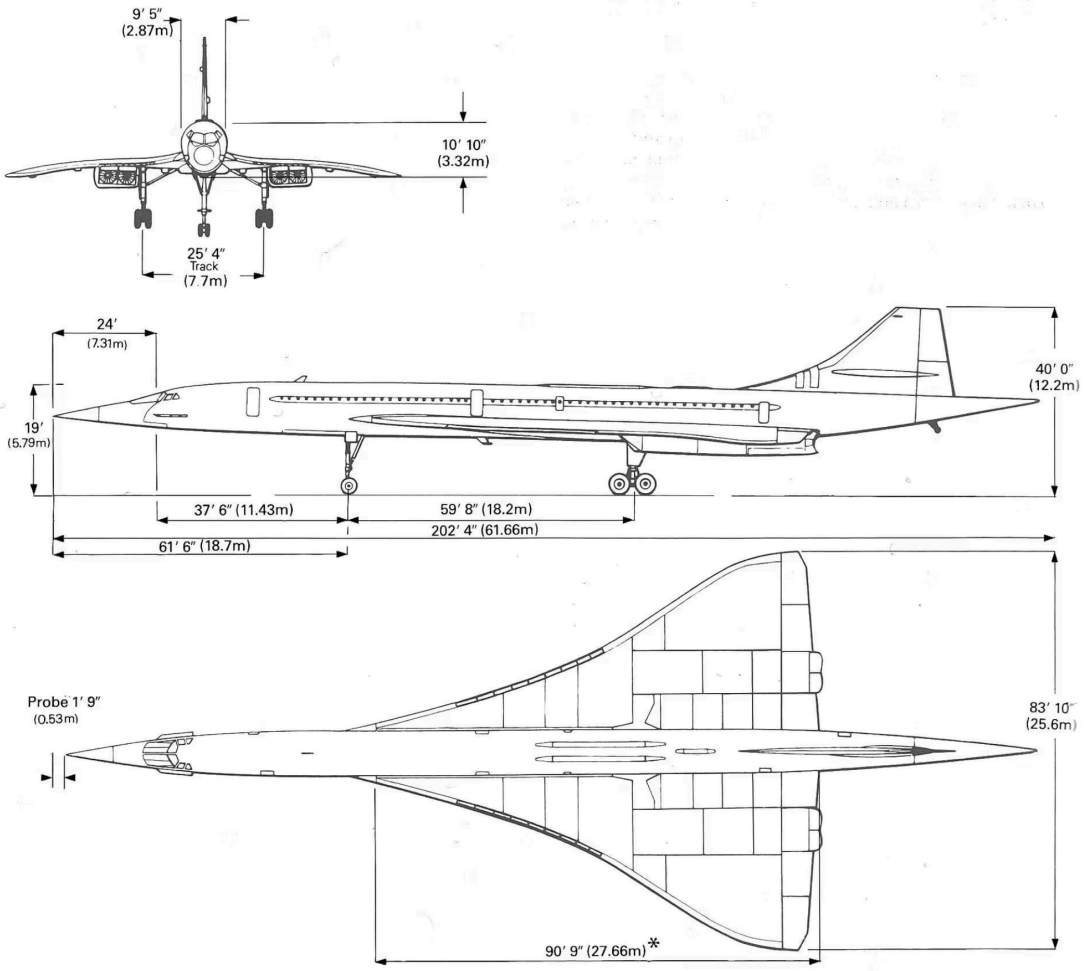

Figure 3.1: Concorde - Aircraft dimensions

3.1.1 Fuselage

The fuselage of the Concorde had an extremely **slender shape**, designed to reduce aerodynamic drag at high supersonic speeds, with a relatively small oval cross-section in order to limit the frontal area and consequently reduce the overall drag.

One of the most well-known features of the Concorde was the **droop nose**, designed to solve the problem of poor visibility during takeoff and landing, due to the large angles

of attack typical of delta-wing aircraft. This allowed the nose to be lowered by up to 12.5° to improve visibility for pilots during takeoff and landing, and raised again during cruise to restore the optimal aerodynamic profile.
The droop-nose system was combined with a **transparent movable visor**, which was retracted during takeoff and landing and closed during cruise flight to protect the windshield from kinetic heating. [Fig.3.2]

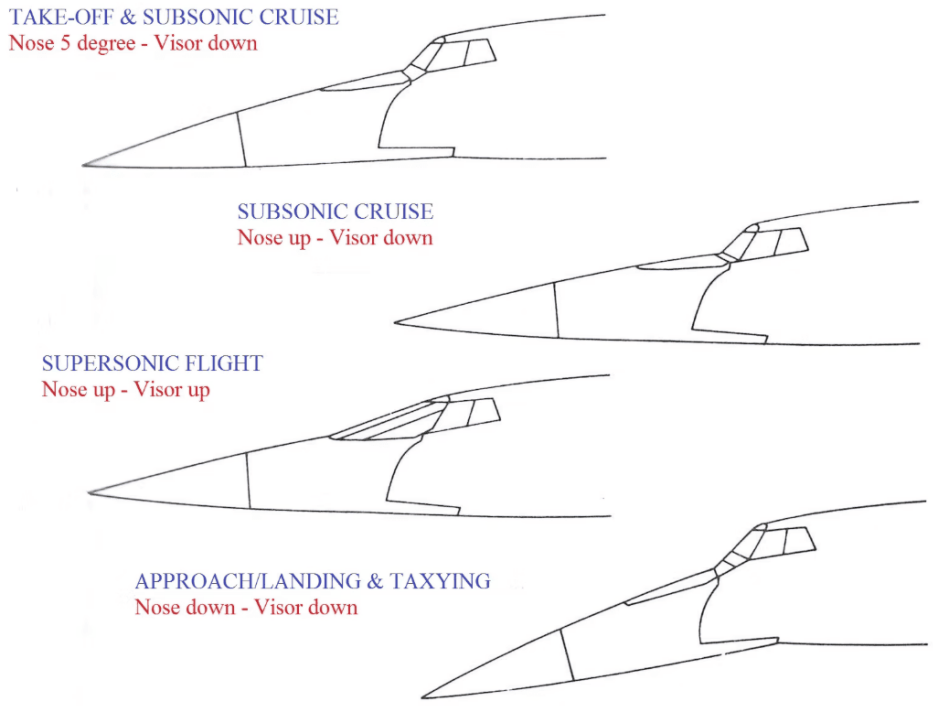

Figure 3.2: Concorde - Drop-nose and visor option [22]

The entire structure was made of high-strength aluminum alloys capable of handling the mechanical and thermal stresses generated by flying at Mach 2. In order to mitigate the effects of heating, the exterior paint was highly reflective white, which reduced heat absorption and helped keep surface temperatures within acceptable limits.

3.1.2 Wing and Tail Configuration

The wing of the Concorde adopted an **ogival delta** configuration, which is a typical aerodynamic choice for supersonic aircraft, as it reduces wave drag while maintaining good efficiency at high speeds and, thanks to the ogival profile of the leading edge, provides a more uniform lift distribution and better stability at low speeds. 3.3

Due to the absence of conventional flaps, the aircraft had to generate the necessary lift only through the aerodynamics of the delta wing, using the phenomenon of **vortex lift**: at low Mach numbers and high angles of attack, vortices along the leading edge contributed to increasing lift and delaying stall, allowing for safe takeoff and landing operations despite the geometry optimized for supersonic flight.

In Fig.3.4 the strong conical vortex forms over the leading edge of the delta wing can be seen by vapour condensation.

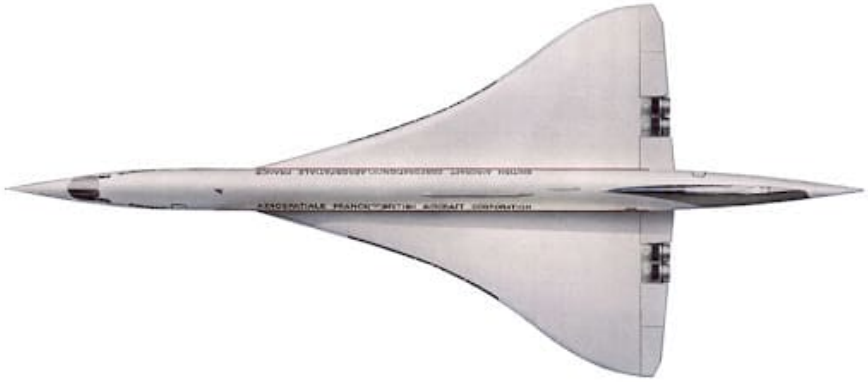

Figure 3.3: Concorde - Delta Wing

Figure 3.4: Phenomenon of vortex lift [22]

The main control surfaces were integrated along the trailing edge of the wing and consisted of six **elevons** (three per wing half), which combine the functions of both elevators and ailerons to control pitch and roll.
On the other hand, the tail had no horizontal tail planes, and the only element present was the **vertical fin** with a split rudder, which ensured yaw control and directional stability at high speeds.

3.1.3 Engines

The Concorde was equipped with four **Rolls-Royce/Snecma Olympus 593 Mk610** engines, specifically designed to guarantee high performance in supersonic cruise mode,

at around Mach 2. [Fig.3.5]
Each engine was capable of providing approximately 169 kN of thrust with active afterburners, giving the aircraft a high thrust-to-weight ratio and remarkable performance for a civil aircraft, but fuel consumption was high in subsonic and climb phases.

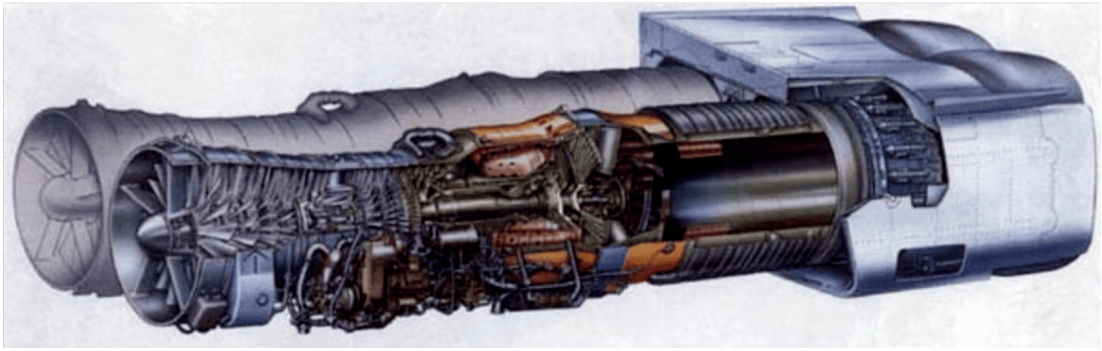

Figure 3.5: Two Concorde Olympus 593 MK.610 engines [22]

General characteristics	
Type	Turbojet
Length	4039 mm (159 in)
Diameter	1212 mm (47.75 in)
Dry weight	3175 kg (7,000 lb)
Performance	
Maximum thrust	wet: 169.2 kN (38,050 lbf); dry: 139.4 kN (31,350 lbf)
Overall pressure ratio	15.5:1
Specific fuel consumption	1.195 (cruise); 1.39 (SL) lb/(h · lbf)
Thrust-to-weight ratio	5.4

Table 3.1: Olympus 593 Mk 610 specifications [22]

The engines were mounted in pairs under the wings, inside nacelles that also incorporated the complex air intake and exhaust systems: [Fig.3.6]

- The air intakes, with variable geometry, used a set of movable ramps and adjustable exhaust doors to slow the flow from supersonic to subsonic speeds before entering the compressor, generating controlled shock waves
- The exhaust was equipped with variable geometry nozzles, composed of movable elements that regulated the expansion of the gases according to the flight phase, to ensure the correct balance between thrust and efficiency.

Afterburning (reheat) was mainly used during takeoff and transonic acceleration to temporarily increase thrust, while it was deactivated during cruise flight to reduce fuel consumption and maintain overall efficiency.

Figure 3.6: Concorde - Engine nacelles [22]

3.1.4 Control surfaces and stability

The control surfaces of the Concorde were designed to ensure control of the aircraft on all three axes and maintain stability over a wide range of speeds and included:

- **six elevons** along the trailing edge of the wing, three per wing, which combined the functions of ailerons and elevators, thus controlling both pitch and roll;
- **two rudders** on the vertical tail, used for yaw control and directional stabilisation at high speeds.

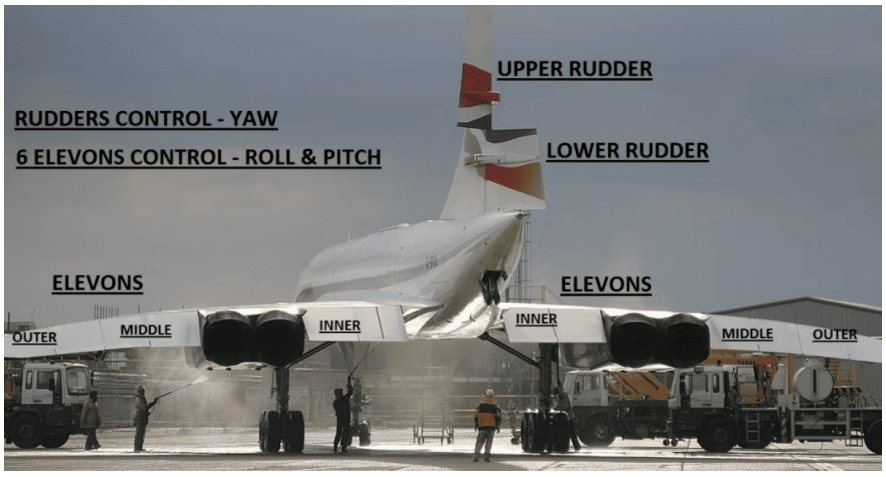

Figure 3.7: Concorde - Control surfaces [22]

In terms of stability and control, the three axes were managed as follows:

- **Pitch**: mainly via the internal elevons, assisted by an automatic trim system that reduced the forces on the controls;
- **Roll**: managed by the external elevons, with integrated compensation logic;
- **Yaw**: handled by the vertical rudders, supported by a yaw damper that dampened any oscillations and ensured directional stability during supersonic flight.

Another key feature of the Concorde was its **centre of gravity management system**: during flight, fuel consumption changed the position of the centre of gravity, affecting balance and aerodynamic drag, so the aircraft was equipped with a complex fuel transfer system between the various tanks to keep the centre of gravity (CG) within optimal limits.
Figure 3.8 illustrates the mechanism: during supersonic cruise, the CG was moved towards the tail, reducing elevon deflection and improving aerodynamic efficiency, while during take-off and landing, the fuel was moved back to a more forward position to ensure greater stability at low speeds.

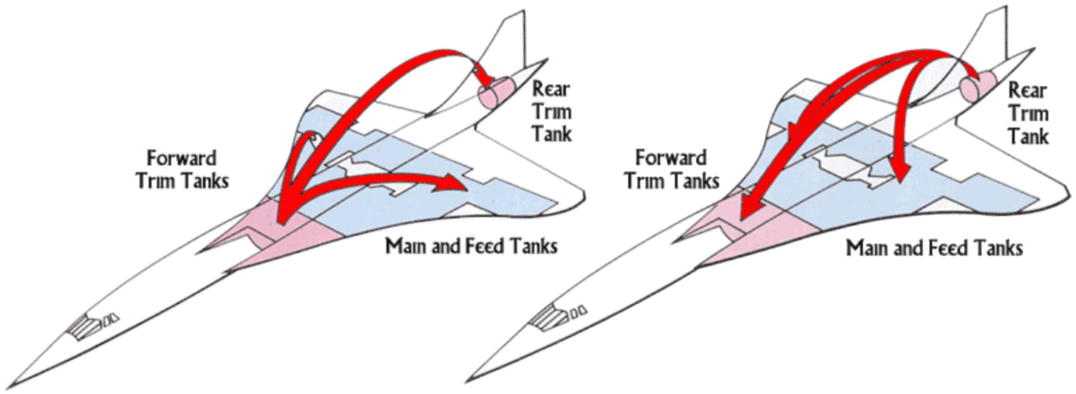

Figure 3.8: Concorde - Fuel transfer

3.2 CS1A

The CS1A is a civil supersonic aircraft designed for a cruising speed of Mach 2, developed as part of the **MORE&LESS** project and derived from the **Concorde-NEO** concept, developed during the *Integrated Aerospace Systems Design* course at the Politecnico di Torino [20], with the aim of exploring aerodynamic and propulsion solutions with reduced environmental impact for high-performance passenger transport.
The configuration was constrained by design requirements, which prescribed an MTOW of less than 200 tonnes, a passenger capacity of approximately 120, and a range of between 7,200 and 9,000 km, greater than that of the Concorde, in order to extend transoceanic routes.

The chosen configuration closely reproduces that of the Concorde, with the following main features:

- an extremely slender fuselage, with a reduced cross-section to minimise the frontal area and limit aerodynamic drag;
- an ogival delta wing, capable of generating additional lift through the vortex lift phenomenon at low speeds and maintaining an optimised aerodynamic profile during cruise;
- the absence of horizontal tail planes, which reduces weight and structural resistance and simplifies the rear of the aircraft;
- pitch and roll control provided by elevons integrated into the wing trailing edge and a vertical rudder for yaw.

From a propulsion point of view, the CS1A keeps a configuration with four engines integrated under the wing, as in the Concorde, but uses an updated version of the Rolls-Royce/Snecma Olympus 593 engine, adapted to modern thrust requirements and technologies. The MORE&LESS project aircraft requires approximately 60 kN of thrust per engine in cruise conditions, so a **scaled-up** version of the Olympus has been developed [Fig. 3.9], featuring increased airflow and diameter, together with higher combustion temperatures and compression ratios.

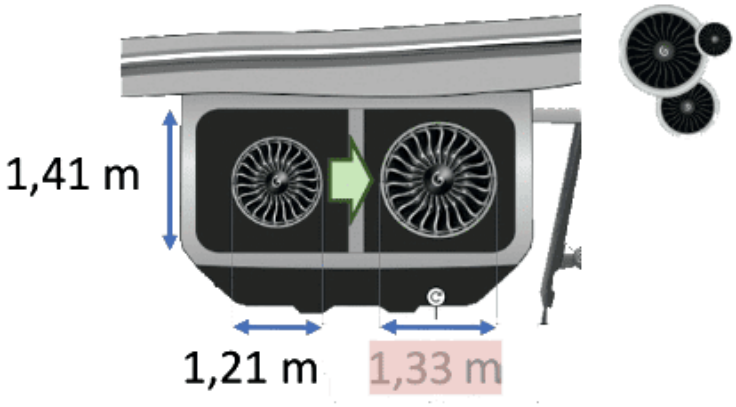

Figure 3.9: CS1A - Scaled-up engine [23]

In terms of size, the CS1A has similar proportions to the Concorde, with a length of approximately 61.7 m, a wingspan of 25.6 m, a wing area of 358 m^2 and a fuselage diameter of approximately 2.9 m.

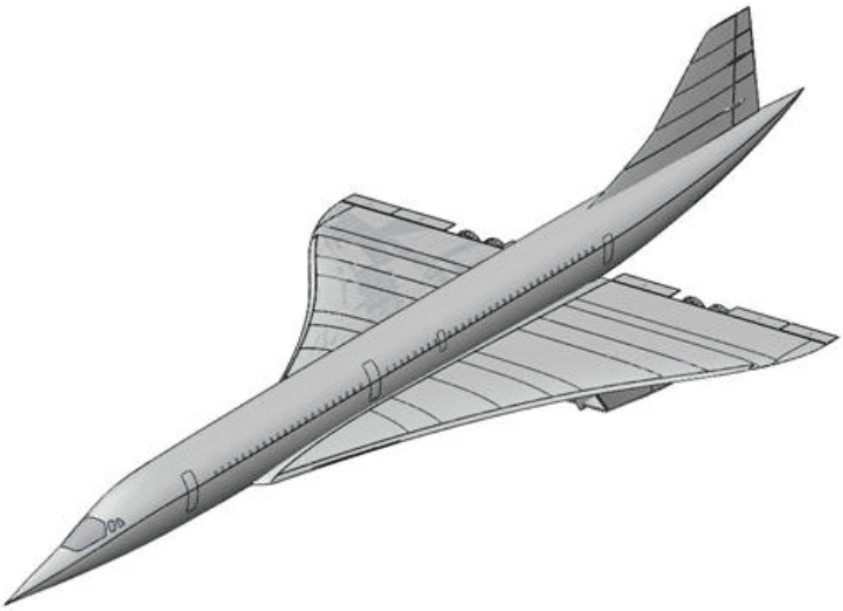

Figure 3.10: CS1A - CAD model [23]

3.3 MODEL ON PLANE MAKER

To create a custom aircraft model for simulation in X-Plane, the program includes **Plane Maker** software, which is not limited to aesthetic representation but allows you to directly define all parameters that affect aerodynamics and flight performance.
The official software manual [24] suggests "a good workflow sequence to start from when modeling in Plane Maker," structured as follows:

1. Decide on a design.
2. Create the fuselage, wings, and tail of the aircraft.
3. Create secondary objects, such as landing gears and engine nacelles.
4. Set up the systems and internal properties, including the engines, electrical systems, weight and balance, and viewpoints.
5. Set up any additional features of the aircraft, such as added weapons or special controls.
6. Create a 2-D instrument panel.
7. Test-fly the aircraft in X-Plane and fine-tune the features of the aircraft from steps 2–6 as needed.
8. Add textures, 3-D objects, extra liveries, etc.

This manual, together with Danklaue's video tutorials available on YouTube [25], was the main reference for creating the model of the aircraft to be simulated and in the following paragraphs the focus will be on the main parts of the aircraft configuration: fuselage, wings and tail with their respective control surfaces, and engine.

3.3.1 Fuselage

The fuselage is the main body of the aircraft and is modeled first, in the *Standard* → *Fuselage* section, where there are three main tabs that allow you to view and modify the shape of the body from different perspectives:

- The **Section** tab shows the fuselage as a series of cross sections (or stations) along the longitudinal axis, each of which defines a portion of the fuselage. Modeling starts from this tab, where a value of about twenty stations is usually used to create a "reference grid" useful for tracing the general shape of the aircraft. [Fig.3.11]

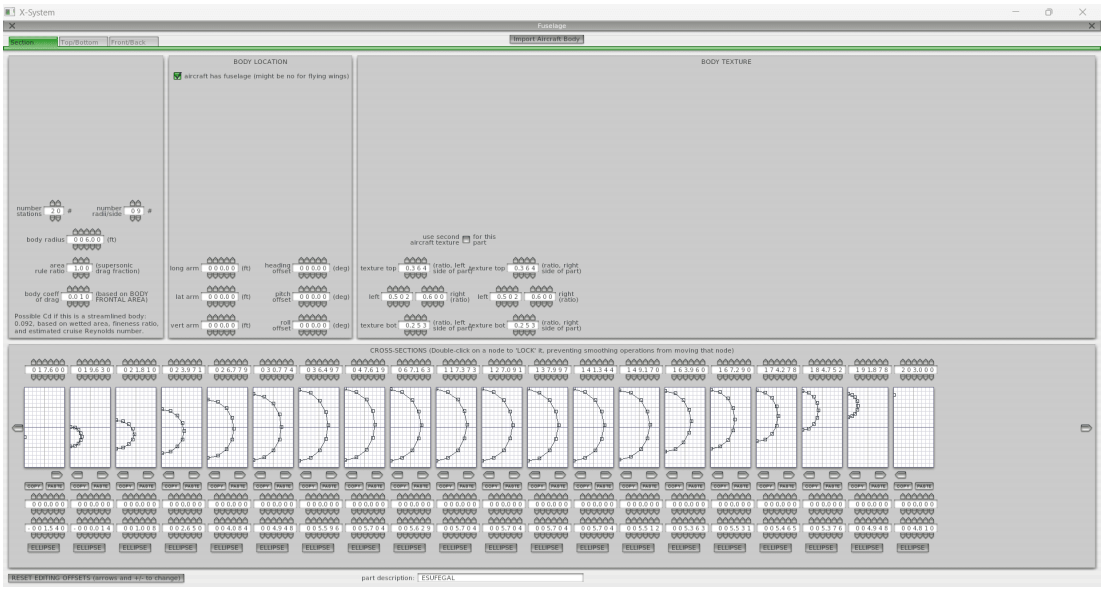

Figure 3.11: Plane Maker - Section tab

- The **Top/Side/Bottom** tab allows you to view the control points defined in the section view from above, from the side, and from below, respectively, and allows you to move them in three-dimensional space to refine the curvature and improve continuity between sections. [Fig.3.12]

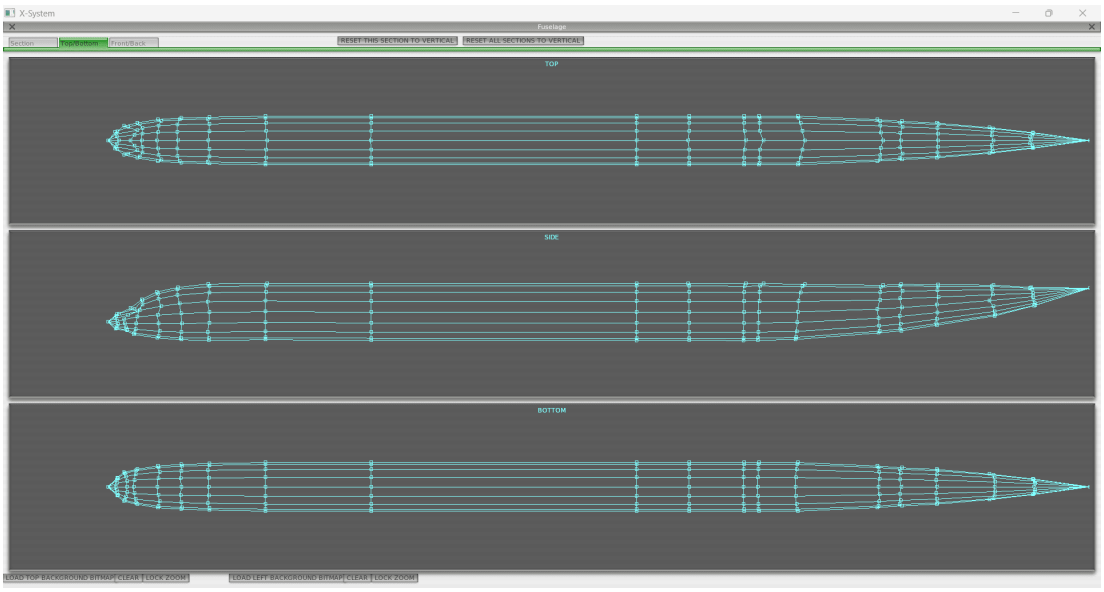

Figure 3.12: Plane Maker - Tob/Side/Bottom tab

- Finally, the **Front/Back** tab shows a front or rear view, which is useful for checking the symmetry of the model and ensuring that the profile is regular. [Fig.3.13]

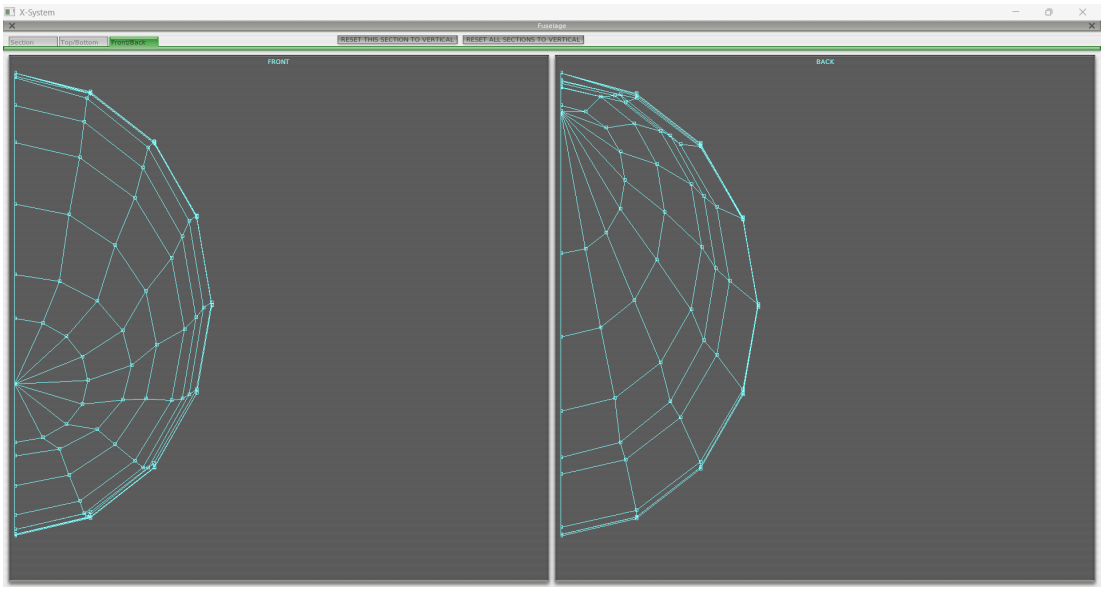

Figure 3.13: Plane Maker - Front/Back tab

In this initial phase, it was very useful to use a reference image as a background, such as a side or top view of the actual aircraft, and to alternate between the different views until obtaining a continuous and proportionate surface.

3.3.2 Wings

The wings are modeled by creating one or more independent sections within the *Standard → Wings / Misc Wings* section, which is divided into three main panels [Fig. 3.14]:

- **Foil Specs**, where you set the geometric characteristics of each section, including the semi-length, root and tip chord, sweep angle, dihedral angle, and position relative to the fuselage;
- **Element Specs**, where the control surfaces are assigned, whose properties are defined in a specific section of the menu (*Standard → Control Geometry*);
- a panel dedicated to the aesthetic aspects of the model, which allows you to refine the texture.

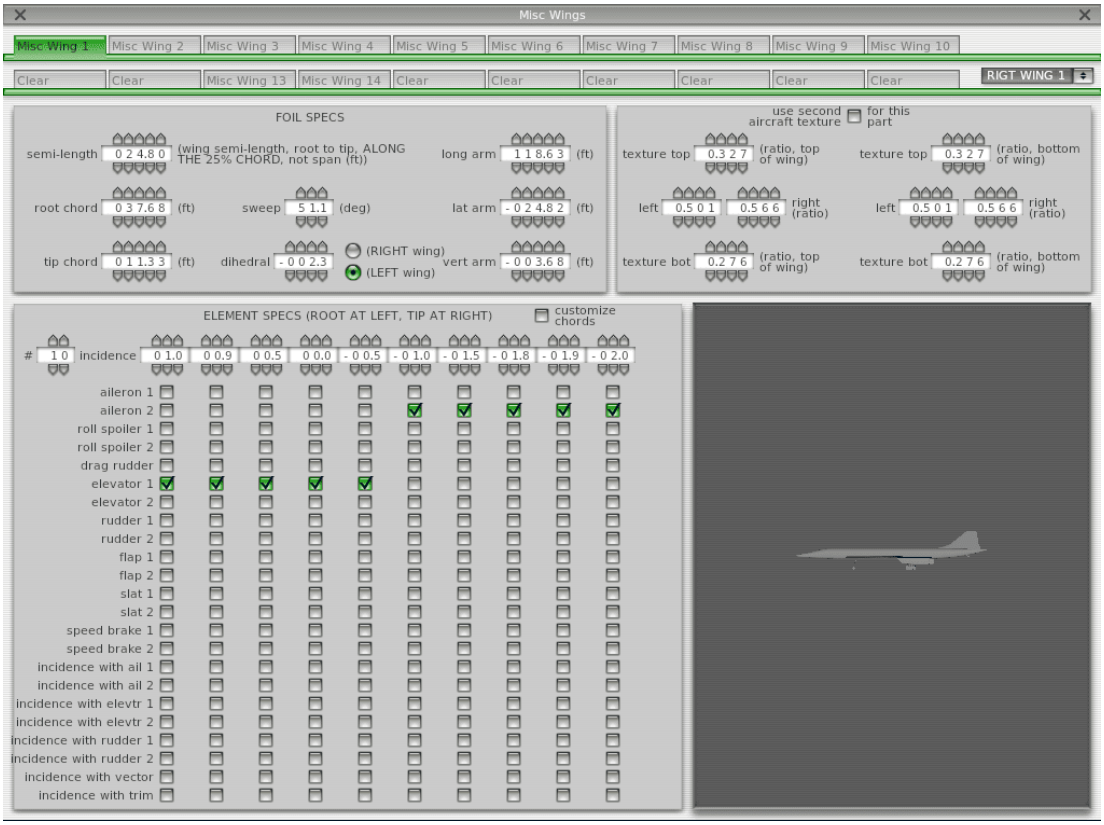

Figure 3.14: Plane Maker - Misc Wings menu

After defining the geometry, we proceed to assign the aerodynamic profile in the *Expert → Airfoils* section, where it is possible to import the airfoil files for the root and tip of the wing. [Fig. 3.15]

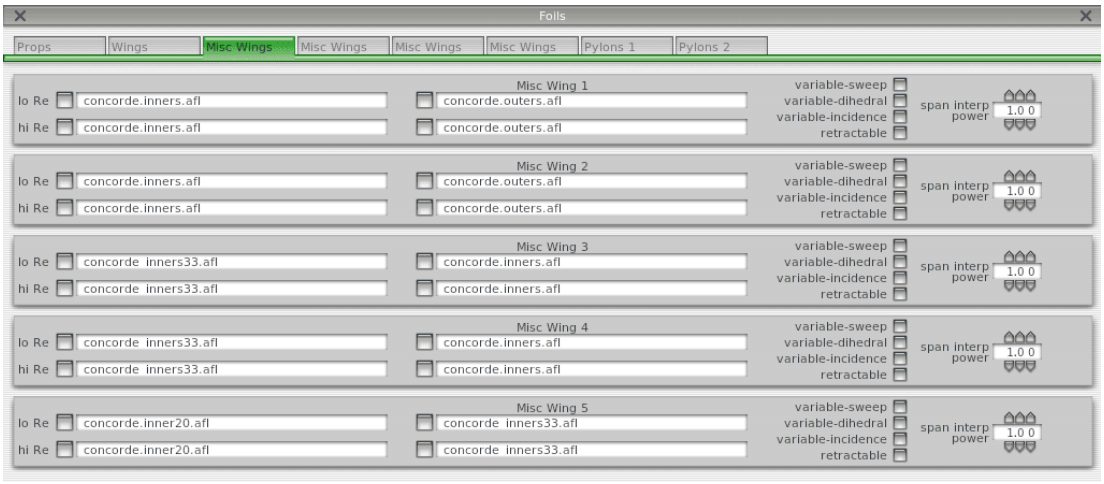

Figure 3.15: Plane Maker - Airfoils menu

In our model, the wings have an ogival delta shape so, to get this shape, we split them into several parts [Fig. 3.16] and, for wings with multiple sections, Plane Maker has a *snap to* feature that makes it easy to automatically align the outer sections with the inner ones, making sure everything flows together.

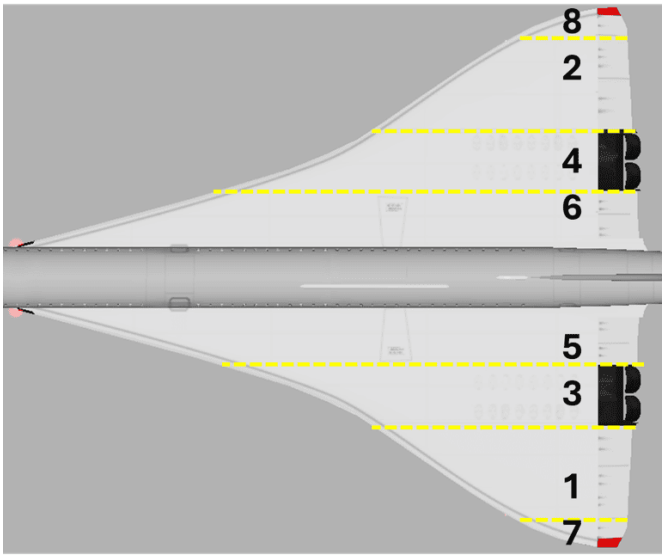

Figure 3.16: Delta Wing model

As described in the previous paragraphs, supersonic aircraft use elevons, which combine the functions of ailerons and elevators, for control surfaces and in Plane Maker they are modeled by selecting both aileron and elevator on the trailing edge of the wing.

Finally, the aerodynamic profiles were found online from a model of the Concorde aircraft.

3.3.3 Tail

The tail is modeled in the *Standard* → *Wings* section, where there are two sections dedicated to vertical stabilizers and one section for the horizontal stabilizer, which are modeled according to the same logic used for the wings, defining the main geometric parameters for each element.

Our model does not have a horizontal stabilizer, as supersonic aircraft generally do not have one, so the tail has been modeled with two vertical stabilizers [Fig. 3.17], to which rudders have been attached as control surfaces, located on the trailing edge.

Figure 3.17: Tail model

3.3.4 Engine

To model the engine, we start by defining the general characteristics in the *Standard* → *Engine Specs* section, where we set the number and type of propulsion engines with their operating parameters and the position of the engines along the three axes.

In the model developed, four jet engines were included, for which we had data on maximum thrust and compressor area, obtained from the diameter, while the number of RPMs was found online [1]. [Fig. 3.18]

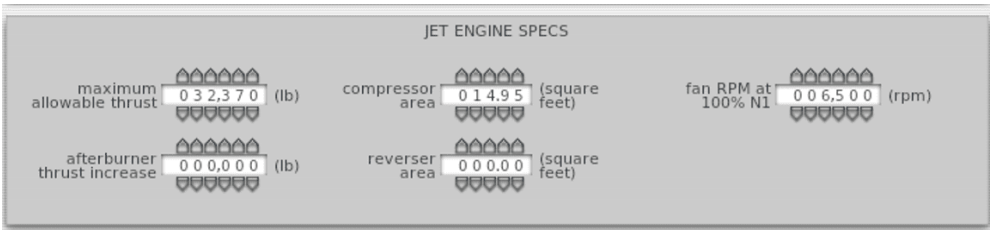

Figure 3.18: Plane Maker - Jet engine specs menu

Next, the structural elements associated with the propulsion system are added,

[1] "At 100% N1 speed, we are at 6500 RPMs" [26]

which are:

- the nacelles, through the *Standard* → *Engine Nacelles* section, which represent the external bodies of the engines to which they are associated and are modeled in an interface similar to that of the fuselage; [Fig. 3.19, 3.20, 3.21]
- the engine pylons, through the *Standard* → *Engine Pylons* section, which are the support structures that connect the engines to the fuselage.

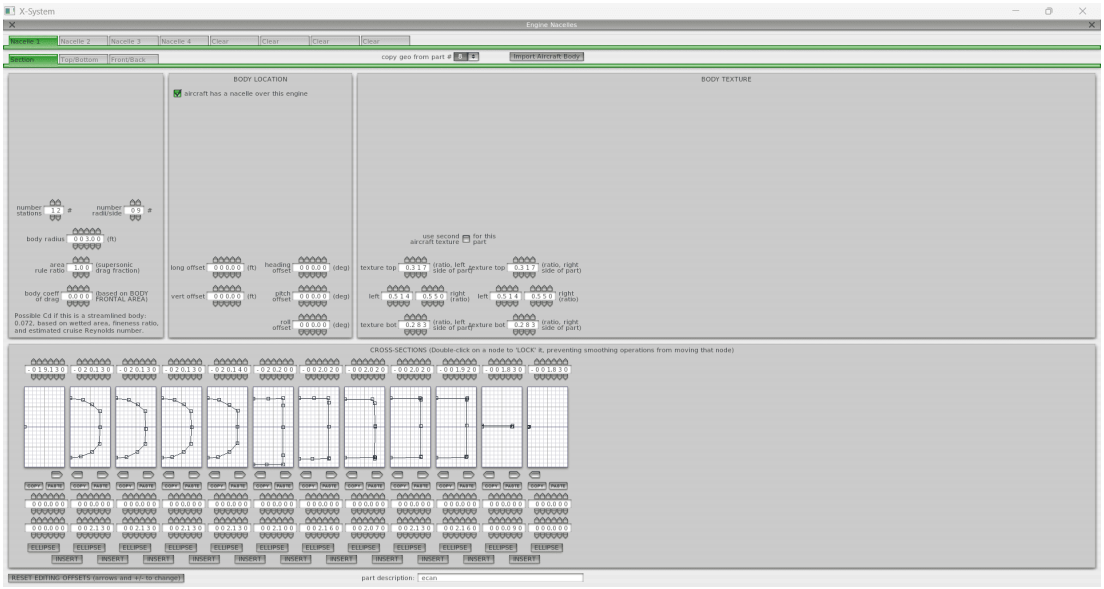

Figure 3.19: Plane Maker - Section tab

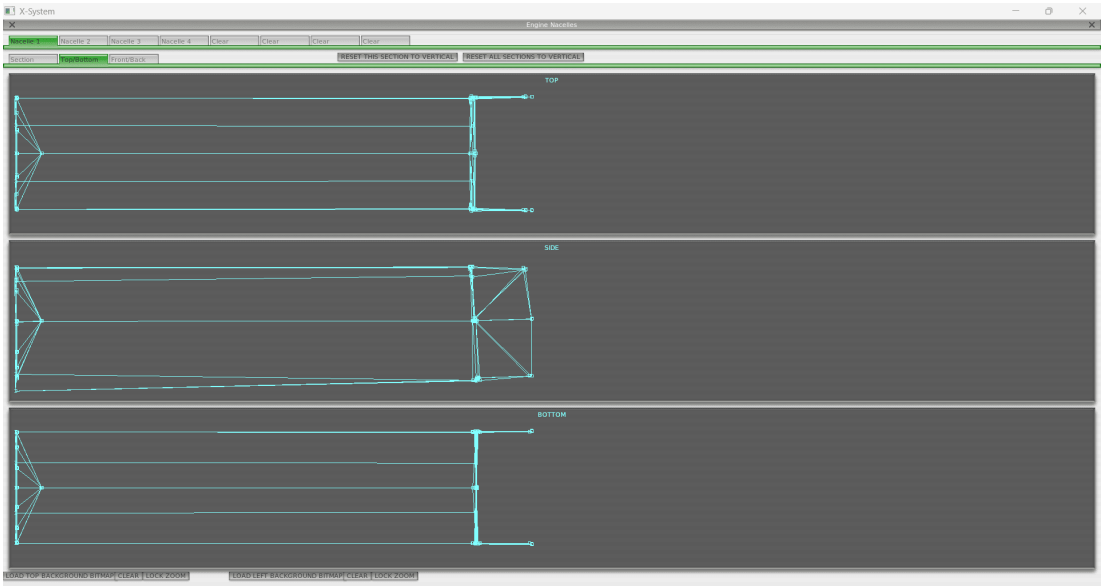

Figure 3.20: Plane Maker - Tob/Side/Bottom tab

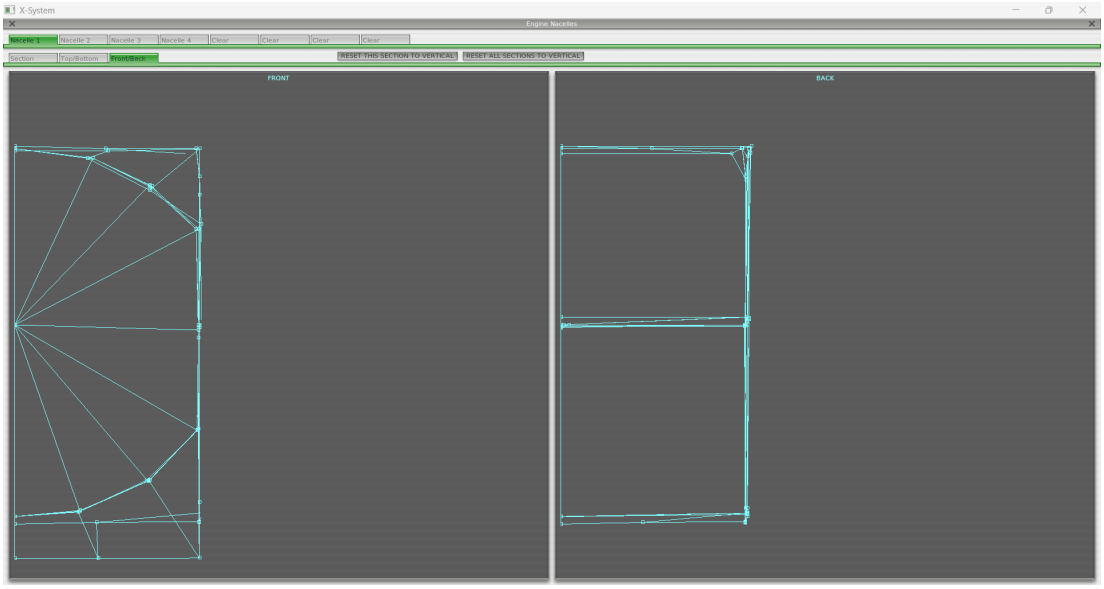

Figure 3.21: Plane Maker - Front/Back tab

The result of the modeling in Plane Maker is shown in Figure 3.22: to improve the visual rendering of the model, .obj files derived from the CAD model of the aircraft were imported into Plane Maker, obtaining a more realistic and less simplified representation than that generated by the software.

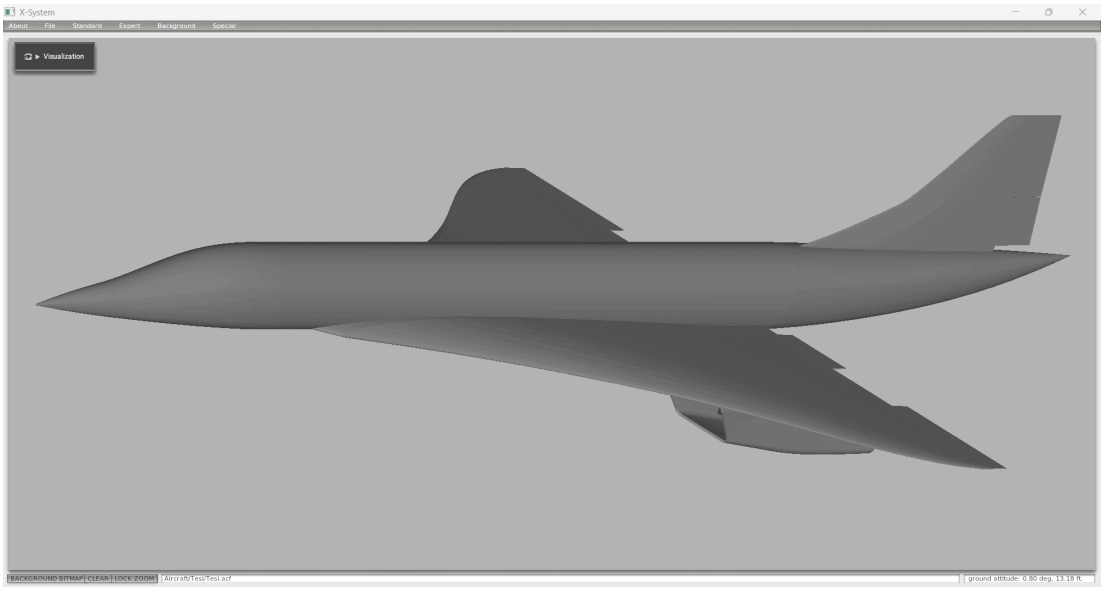

Figure 3.22: CS1A model

Chapter 4

SIMULATIONS

The most accurate way to quantify the environmental impact of an aircraft is to use data from real operations, in particular Flight Data Recorders (FDRs), which are not accessible. Alternatively, ADS-B datasets or radar data could be used, but these do not contain essential information for estimating environmental impact, such as aircraft mass, engine thrust, and flap settings at each point along the flight path.
To overcome these gaps, the study by Askari and Cremaschi [2] proposes an approach based on the use of a flight simulator, X-Plane, to generate radar-type data in which mass, flap configuration, and thrust are known, which are used to train three neural network models capable of estimating the three parameters even when they are not available in real data. Their study focused on a single aircraft (Boeing 747-400) and the results showed that, overall, the method is capable of estimating the three parameters with a reasonable degree of uncertainty, even when using low-quality data.

This chapter will describe the main steps of the method, using the article [2] as the main reference.

4.1 X-PLANE SIMULATOR

Although there are many alternatives among flight simulators, **X-Plane** was chosen for its high precision in simulating aerodynamic behavior.
X-Plane is a professional flight simulator designed to realistically reproduce the dynamics of both fixed-wing and rotary-wing aircraft, and is able to accurately predict the flight characteristics of an aircraft. For this reason, it is also used in training and features in several FAA-certified training programs [27].

The most significant feature, and the main reason why it was adopted in the study by Askari and Cremaschi [2] and therefore in this thesis, concerns the aerodynamic model used by the simulator, namely **Blade Element Theory (BET)**: to calculate aerodynamic forces, the aircraft is divided into a large number of elementary sections and the aerodynamic forces on each of them are calculated before being recomposed on the entire structure.

This method allows to obtain accurate flight dynamics in subsonic and, in part, transonic conditions, with performance comparable to more complex techniques such as computational fluid dynamics, but with much lower computational costs. [28]

Another distinctive feature of X-Plane is the ability to communicate with the simulator in real time using the **User Datagram Protocol (UDP)**, which allows you to read and modify a wide range of internal variables, thus enabling you to control the simulation from the outside in an accurate and programmable manner.
Communication with external software such as Python is achieved through the open-source **X-Plane Connect (XPC) plugin**, developed by NASA, which provides dedicated functions for transferring data and sending commands to the simulator in real time. [2]

The starting point for generating simulations is the construction of the aircraft using the integrated **Plane Maker** software, which allows you to define geometry, masses, control surfaces, and propulsion characteristics, as discussed in the previous chapter (3).

4.2 DATA GENERATION

The generation of simulated data is the central phase of the methodology, as the flights generated with X-Plane have a dual purpose: the first set consists of **training data**, used to train neural network models, which are then tested on a test data set; once the training phase is complete, the test set is converted into **surveillance format data**, reproducing the characteristics of ADS-B and radar data, so that the performance of the models can be estimated more realistically and their behavior when applied to data from real flights can be replicated. [2]

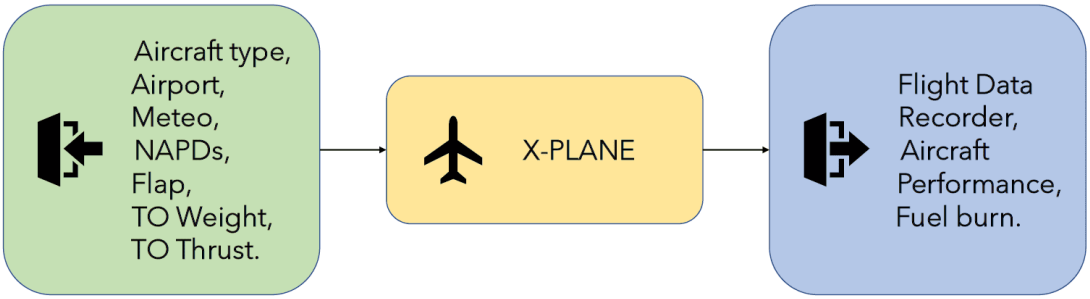

Figure 4.1: Generate X-Plane flights (©ENVISA)

The data generation process is based on controlled variability in simulations: each

scenario reproduces a realistic takeoff procedure, randomly selected from those contained in ICAO document 9888 [29], and each relevant operating parameter that influences the takeoff profile is randomized according to realistic intervals. Weather conditions also vary within operational limits, including sea level temperature and pressure, wind speed and direction, and runway conditions (dry, damp, or wet).
Table 4.1 summarizes the variability of the main parameters considered in the simulations.

Variable	**Range / Distribution**
End altitude	±2% of nominal value
End calibrated airspeed	±5% of nominal value
Climb angle reduction during acceleration	±20%
Sea level temperature	-5 °C – 30 °C
Sea level pressure	0.97 – 1.03 atm
Wind speed at 4000 m	0 – 23.15 m/s
(X-Plane automatically generates the vertical profile interpolating between wind layers)	
Wind direction	Runway heading ±45°
(Non-uniform distribution centered on runway heading)	
Runway condition	50% dry, 25% damp, 25% wet

Table 4.1: Variation ranges of the main variables in the take-off simulations [2]

Takeoff and the following climb phases are divided into four main segments:

- Takeoff
- First Climb
- Acceleration
- Second Climb

Each one of these phases is implemented in X-Plane to generate realistic trajectories, with particular attention to the use of PID controllers, filters, and control logic used to control trim, thrust, and control surfaces.

4.2.1 Take off

The takeoff phase represents the initial moment of flight, including both the takeoff run and the separation from the runway.
In this phase, the simulation in X-Plane initially involves the selection of **flap configuration**, chosen from the aircraft's operating options, on the basis of which the critical takeoff speeds are calculated, including rotation speed (V_R) and climb safety speed (V_2). Then, a slight variability is added to the critical speeds to introduce differences between simulated flights, reflecting the natural variability of real processes.
It is important to note that this method [2] was originally tested on a subsonic aircraft (Boeing 747-400), so for this thesis, which focuses on a supersonic aircraft similar to the

Concorde, the methodology has been appropriately adapted, as flaps are not present as control surfaces.

During takeoff, engine thrust adjustment is essential, particularly in terms of **thrust reduction**: pilots do not use the maximum thrust available for takeoff in order to reduce fuel consumption and emissions and decrease engine wear, but follow reduced thrust guidelines provided by airlines based on variables such as takeoff weight, runway conditions, and weather conditions.
To replicate this behavior in X-Plane, each simulation introduces a random reduction in thrust relative to the aircraft's maximum rated value, thus generating a variety of takeoff profiles consistent with operational reality.

This reduction is implemented using a **throttle PID controller**, which compares the actual thrust of the engines with the desired thrust in real time and calculates the corrections needed to the throttle to reach the target value.

$$Thrust_c^{[k]} = Thrust_d \frac{dt}{T} + \frac{1 - dt}{T} Thrust_c^{[k-1]} \tag{4.1}$$

$$Thrust_e^{[k]} = \frac{Thrust_c^{[k]} - Thrust^{[k]}}{Thrust_c^{[k]}} \tag{4.2}$$

$$\text{Throttle}^{[k]} = \text{Throttle}^{[k-1]} + k_p \text{Thrust}_e^{[k]} + k_d \frac{\text{Thrust}_e^{[k]} - \text{Thrust}_e^{[k-1]}}{dt} + k_i \int \text{Thrust}_e dt \tag{4.3}$$

In the above equations, $Thrust_c$ indicates the commanded thrust, while $Thrust_d$ represents the desired thrust calculated based on the expected reduction for the takeoff phase. To avoid overly rapid changes or unwanted oscillations, the command is filtered using a time constant T. The simulation time interval is dt, and $[k]$ indicates the k-th step. The PID controller parameters (k_p, k_i, k_d) are calibrated through iterative testing in order to obtain a stable response consistent with the aircraft's dynamics.

In addition, to maintain alignment with the runway in the presence of crosswinds, another PID controller is implemented, called **rudder control**, which evaluates the error between the desired heading and the actual heading of the aircraft and controls the rudder surface.

$$\psi_e = \psi_d - \psi \tag{4.4}$$

$$\text{Rudder} = k_p \psi_e + k_d \frac{d(\psi_e)}{dt} + k_i \int \psi_e \, dt \tag{4.5}$$

4.2.2 First Climb

The next phase is the First Climb, in which the main objective is to maintain a constant calibrated speed, controlling the angle of climb via the elevator control surface, whose deflection is determined by estimating the error between the desired angle of climb and the actual angle of the aircraft.

Assuming, as a first approximation, that the ground speed must remain constant, the equations of motion can be expressed as:

$$T\cos(\alpha) - D - mg\sin(\gamma) = ma \tag{4.6}$$

$$T\cos(\alpha) - D - mg\sin(\gamma + \Delta\gamma) = 0 \tag{4.7}$$

where T is the total thrust, a is the change in ground speed, α is the angle between the thrust vector and the flight path, g is gravity, m is the mass of the aircraft, D is aerodynamic drag, and γ is the angle of climb.

Subtracting the two equations gives:

$$g\sin(\gamma) + a - g\sin(\gamma + \Delta\gamma) = 0 \tag{4.8}$$

$$g\sin(\gamma) + a - g\sin(\gamma)\cos(\Delta\gamma) - g\cos(\gamma)\sin(\Delta\gamma) = 0 \tag{4.9}$$

Considering the variation $\Delta\gamma$ to be small ($\cos(\Delta\gamma) \approx 1$, $\sin(\Delta\gamma) \approx \Delta\gamma$), we can obtain an estimate of the necessary variation in the angle of climb, which will then be used as a reference for the PID controller:

$$\Delta\gamma = \frac{a}{g\cos(\gamma)} \tag{4.10}$$

To maintain a constant calibrated speed, an **elevator control** based on a PID controller is implemented.

$$\gamma_d^{[k]} = \gamma^{[k]} + \Delta\gamma^{[k]} \tag{4.11}$$

$$\gamma_c^{[k]} = \gamma_d^{[k]}\frac{dt}{T_\gamma} + \gamma_c^{[k-1]}\frac{1 - dt}{T_\gamma} \tag{4.12}$$

$$\gamma_e^{k} = \gamma_c^{[k]} - \gamma^{[k]} \tag{4.13}$$

$$\text{Elevator}^{[k]} = k_p\gamma_e^{[k]} + k_d\frac{\gamma_e^{[k]} - \gamma_e^{[k-1]}}{dt} + k_i\int \gamma_e\, dt \tag{4.14}$$

In these equations, γ_d, γ_c and γ_e represent the desired value, the commanded value and the climb angle error, respectively. In this case too, a filter with a relatively high time constant T_g is introduced, which is useful for avoiding oscillations or instability due to dynamic delays in the system: in fact, the variation in the elevator first causes a change in attitude, then in lift, and finally in the angle of climb.

In addition to elevator control, **roll control** is also implemented, again using a PID applied to the ailerons, which evaluates the error between the desired bank angle and the actual bank angle to calculate the deflection of the surfaces required to stabilize the aircraft during climb.

$$\phi_e = \phi_d - \phi \tag{4.15}$$

$$\text{Aileron} = k_p\phi_e + k_d\frac{d(\phi_e)}{dt} + k_i\int \phi_e\, dt \tag{4.16}$$

4.2.3 Acceleration

During the acceleration phase, the goal is to gradually reduce the angle of climb to allow for an increase in speed. For this reason, the desired angle of climb, calculated in the previous phase, is reduced by a fixed percentage within a predetermined range in order to obtain a realistic acceleration profile.

At this stage, an **elevator PID controller** is implemented, which receives the attitude error as input and returns the deflection necessary to quickly converge the actual angle of climb to the commanded angle.

$$\gamma_c^{[k]} = \gamma_d^{[k]} \frac{dt}{T_\gamma} + \gamma_c^{[k-1]} \frac{1 - dt}{T_\gamma} \tag{4.17}$$

$$Elevator^{[k]} = k_p \gamma_e^{[k]} + k_d \frac{\gamma_e^{[k]} - \gamma_e^{[k-1]}}{dt} + k_i \int \gamma_e \, dt \tag{4.18}$$

The filter applied to the controlled corner has a faster time constant than that used in the first climb, as the duration of this segment is shorter and requires a more immediate dynamic response.

The method [2] also involves the progressive **retraction of the flaps**: each flap configuration is associated with a maximum speed, and when the aircraft exceeds this value, the system automatically switches to the next, less extended configuration; once the speed limit for the next step is reached, the flaps are retracted further, and so on.
However, for the Concorde, this logic is not applied because the aircraft does not use traditional flaps.

Finally, if required by the noise abatement procedure, a **throttle reduction** within a defined range may be applied at this stage; without such constraints, thrust is kept constant in continuity with the previous phase.

4.2.4 Second Climb

In the final phase, the second climb, the control logic maintains the same structure adopted in the First Climb: the algorithms used to control the **angle of climb** and **banking** remain identical, but the gains are properly modified to adapt to the new speed conditions.

Another difference concerns the use of the **throttle controller**, which, 5 seconds after the start of the second climb, adjusts the throttle to keep the engine power constant over time.
In this case too, the controller is of the PID type, but unlike the previous segments, no filter is applied to the command, since the thrust variation is gradual and does not require additional damping to ensure system stability.

$$Power_e^{[k]} = Power_d^{[k]} - Power^{[k]} \tag{4.19}$$

$$Throttle^{[k]} = Throttle^{[k-1]} + k_p Power_e^{[k]} + k_d \frac{Power_e^{[k]} - Power_e^{[k-1]}}{dt} + k_i \int Power_e \, dt \tag{4.20}$$

4.3 NEURAL NETWORK MODELS

The data generation process described in the previous chapter provides sufficient information for training neural network models. Specifically, **three multilayer perceptron (MLP) neural network models** were developed, each with a specific objective: estimating aircraft weight, estimating thrust, and predicting flap position.

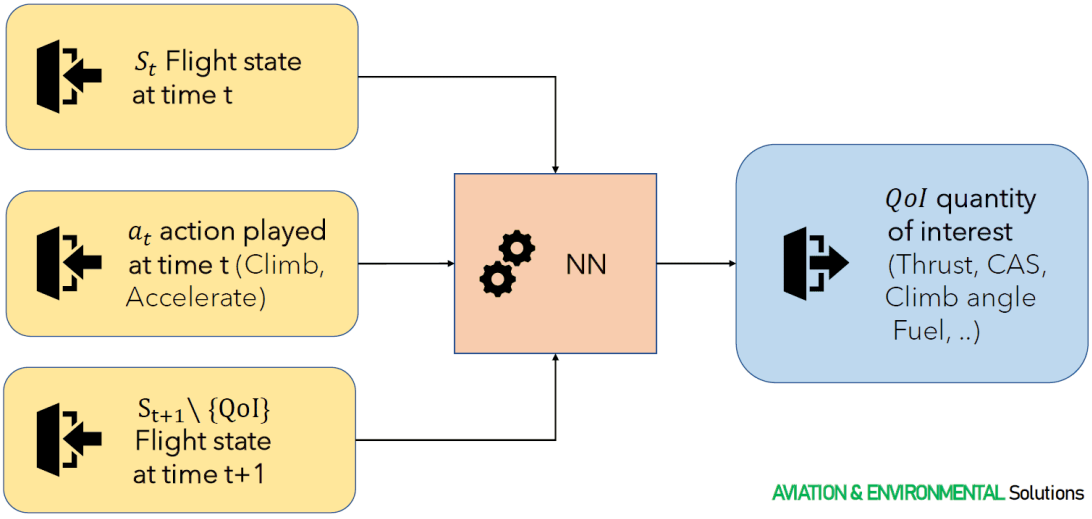

Figure 4.2: Replicate the aircraft performance model using NN (©ENVISA)

4.3.1 Weight model

This model uses inputs from different segments of the flight, but in order to ensure the accuracy of the estimate, the takeoff phase is not included among the inputs, as in actual surveillance data this phase is often under-represented and difficult to distinguish from the taxiing phase.
Although the data generated by X-Plane contains all the necessary information on this phase, it was decided to exclude it in order to focus the model solely on data accessible via the ADS-B format.

The inputs selected for the model include variables averaged over three segments of the flight:

- First Climb: calibrated speed, angle of climb, roll angle, and weather conditions;
- Maximum acceleration segment: angle of climb, roll angle, acceleration, and weather conditions;

- Second Climb: calibrated speed, angle of climb, roll angle, and weather conditions.

The model architecture includes two hidden layers with 32 neurons each, each equipped with a ReLU activation function [1] and an output node that returns the estimated total weight of the aircraft. To reduce the risk of overfitting, a dropout layer with a 3% drop probability was added after each hidden layer.
The network was trained in three consecutive sessions with decreasing learning rates (0.01, 0.001, and 0.0001): initially, higher values are used to allow the model to quickly explore the parameter space, while lower values in the subsequent phases refine the network.

4.3.2 Thrust model

This model uses both the weight estimated by the previous model and other key variables measured during flight as inputs, including ground speed, altitude above ground, acceleration, temperature, air pressure and density, angle of climb, roll angle, wind speed, and the angle between the wind direction and the aircraft's course.

The model architecture includes an input layer composed of 12 variables, four hidden layers with 64, 64, 32, and 16 neurons each, equipped with a sigmoid activation function [2] and an output node that returns the estimated correct thrust.
Network training was performed in three consecutive sessions with decreasing learning rates (0.01, 0.001, and 0.0001). However, unlike the weight model, training was performed on each point of the flight rather than on segment averages, allowing a much larger data set to be exploited and improving the model's ability to generalize on new data.

4.3.3 Flap model

Although supersonic aircraft such as the Concorde are not equipped with traditional flaps, the model description is presented for completeness and to illustrate the procedure followed in the original implementation, based on data from a subsonic aircraft.

The model uses the same variables as input as those used in the thrust model and passes through three hidden layers with 128, 64, and 32 neurons, each with a sigmoid activation function. To prevent overfitting, a dropout layer with a 10% drop probability was added after each hidden layer. The output layer consists of six nodes, each representing a possible flap position, including a transition position for when the flaps

[1] **ReLU** returns zero for negative values and the input value itself for positive ones. It is the default choice for feedforward networks because it introduces non-linearity while keeping the structure simple, which makes optimization with gradient-based methods easier. It helps mitigate the issue of very small gradients (which slow down learning) and allows faster convergence compared to sigmoid functions. [30]

[2] **Sigmoid** compresses the input into the range (0,1), making it useful for representing probabilities. It is chosen to keep values within defined limits and ensure numerical stability. However, it tends to saturate for very large or very small inputs, which reduces learning speed because gradients become almost zero. [30]

are retracted, and output activation is handled by a softmax function [3].
Training was performed in three consecutive sessions with decreasing learning rates (0.1, 0.01, and 0.001). To replicate the surveillance data more realistically, the flap predictions during acceleration segments are averaged over 12-second time windows, while at the end of each acceleration segment the flap value is set to zero.

4.4 VALIDATION

The decision to adopt this methodology for this thesis was supported by the fact that it showed reliable results during the validation analyses carried out in [2]

Once the three neural models had been defined and trained, the main objective was to verify whether these models, developed in a controlled environment, were actually capable of generalizing to noisier and less complete data, as occurs in operational applications. To carry out this validation phase, the data generated by the simulator was transformed to replicate the format and typical quality of ADS-B and radar measurements.

The results showed that the methodology maintains good predictive ability, returning consistent estimates, thus demonstrating that the combined use of high-fidelity simulations and neural networks is a valid alternative for obtaining aerodynamic and propulsion parameters that are not accessible from Flight Data Recorders or other high-precision on-board sensors.

This approach opens up the possibility of extending the methodology to supersonic aircraft such as the Concorde or similar.
In this thesis, an attempt was made to apply the method to such aircraft, which required specific adjustments to the code; these modifications and the corresponding results are discussed in Chapter 6.

[3] **Softmax** converts a vector of values into a probability distribution that sums to 1, allowing each output to be interpreted as the "likelihood" of belonging to a class. It is a generalized version of the sigmoid for problems with more than two categories and is the standard for multi-class classification tasks. [30]

Chapter 5

OPTIMIZATION

An important issue that the aviation community has been dealing with in recent years concerns the noise generated by aircraft operations for communities around airports and the adoption of NADP procedures alone is not enough, because they do not define all the parameters that have a significant impact on ground noise during takeoff.
The neural network approach, presented in the previous chapter, overcomes these gaps so is a valuable tool for conducting environmental assessments of this type, such as the one proposed by Paki et al. in *"Vertical profile noise optimization for aircraft departures using Flight Data Recorder-like data"*. [31]

In this paper, as well as in this chapter, an optimization algorithm is proposed to continuously improve vertical profiles previously generated with neural networks for noise minimization; however, the method is potentially applicable to any other desired objective, such as reducing fuel consumption or emissions.

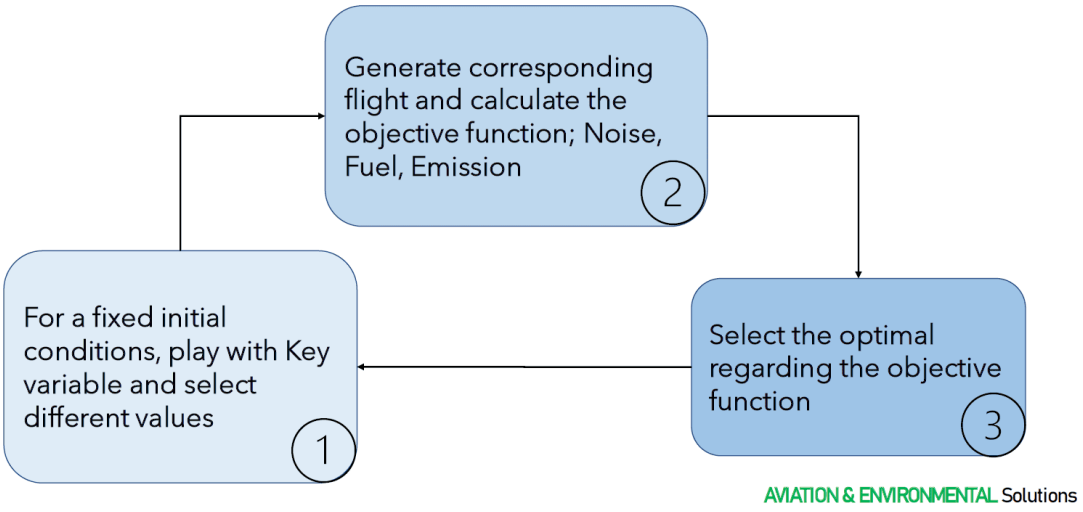

Figure 5.1: Find the optimal profiles to minimize a certain objective (©ENV-ISA)

5.1 DATA GENERATION

To generate realistic profiles, the neural network-based predictive model receives two sets of inputs: initial conditions (S) and controllable variables (X).

The **initial conditions** consists of parameters that define the operating scenario and have been randomly varied to ensure a wide range of scenarios (see Table 4.1 in section 4.2), but cannot be modified during optimization. These include:

- Takeoff weight
- Weather conditions (temperature, pressure, wind)
- Runway conditions (dry, damp, wet)
- Initial configuration (flap setting, runway heading)

Instead, the **controllable variables** derive from the objective of the work, i.e., identifying the optimal vertical profile in terms of noise reduction; they are therefore the optimizable parameters that are modified iteratively by the algorithm.
Assuming that they are all freely adjustable by the pilot, they include:

- Thrust at takeoff;
- End of first step altitude;
- End of second step altitude;
- Cutback thrust;
- Reduction in climb angle during acceleration;
- Maximum CAS speed after acceleration.

All six of these variables have limits to ensure both valid flight trajectories and compliance with aeronautical standards.

Both sets of variables are provided as input to neural networks, which generate trajectories capable of faithfully reproducing real flight situations, returning with high accuracy parameters such as:

- climb angle,
- thrust in the various segments,
- distance covered,
- speed,
- fuel consumption.

5.2 NOISE CALCULATION

To assess the noise impact of the flight profiles generated, the **L_{Amax} metric** [1] was adopted, which represents the maximum sound level perceived during a single takeoff event and is used for comparing the noise impact of two different trajectories when assessing a change of routing (noise impact analysis).

The calculation was performed in accordance with ECAC Doc 29 guidelines [6] and the NPD (Noise-Power-Distance) curves from the Aircraft Noise and Performance (ANP) database [11], which correlate engine power and the distance between the aircraft and the receiver with the perceived noise level on the ground.

For each profile, noise levels are calculated at multiple ground locations selected within the areas of interest to ensure adequate coverage and to evaluate the acoustic impact more realistically than methods that consider only a single observation point.

5.3 DETERMINATION OF OPTIMUM PROFILE

Initially, to generate vertical profiles, controllable flight parameters are defined randomly using the Latin Hypercube Sampling (LHS) method, which ensures good dispersion of samples, avoiding concentrations in particular regions of space.
Subsequently, these parameters are integrated with the initial conditions and modified iteratively to generate new trajectories until the ideal vertical profile is achieved. [Fig. 5.2]

As mentioned in the previous paragraph, there is more than one area of interest in which noise should be minimized, so the problem is defined as multi-objective.
For this reason, it was decided to adopt the **NSGA-II (Non-dominated Sorting Genetic Algorithm II) algorithm** [32], designed for problems in which there is no single optimal solution, but rather a set of compromise solutions, called the Pareto front.
The algorithm uses an evolving approach based on:

- **Nondominated sorting** to classify solutions into Pareto fronts:
  Each solution is evaluated in comparison to the others and obtains a nondominance rank, which indicates how "good" it is considering all objectives together. The solutions on the first front, meaning those that are not dominated by any other, are the best possible in terms of compromise between objectives.

- **Crowding distance** to maintain diversity among solutions:

[1] "The A-weighting is a simple filter applied to sound measurements which applies more or less emphasis to different frequencies to mirror the frequency sensitivity of the human ear at moderate sound energy levels. A-weighted sound level is an almost universally used scale of environmental noise level: it is used for most aircraft noise monitoring applications as well as for the description of road, rail and industrial noise. A-weighted levels are usually denoted as L_A." [6]

The local density around each solution is estimated, allowing NSGA-II to distribute solutions evenly along the Pareto Front and avoid excessive aggregation.

- **Elitism** to preserve the best solutions:
  To avoid losing the best solutions while the algorithm continues to explore the solution space, NSGA-II combines the parent population with the offspring population, selecting the best solutions based on both quality and diversity.

Based on these principles, NSGA-II iteratively evolves solutions until it identifies the optimal vertical profile that minimizes noise in all areas of interest considered.

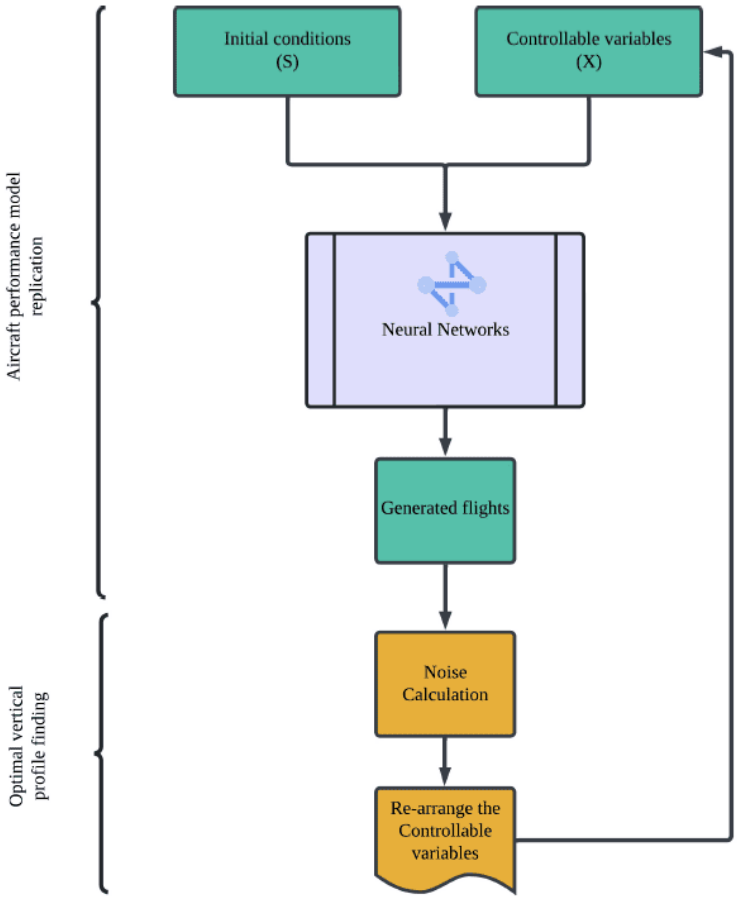

Figure 5.2: Optimal vertical profile finding process [31]

Chapter 6

RESULTS

The use of the Concorde model turned out to be particularly challenging, as it required numerous interventions and modifications to the original code, as illustrated in section 6.1.
In the end, thanks to the corrections, the aircraft was controlled correctly and approximately 4,000 flights were generated. However, the difficulties encountered raised doubts about the accuracy of the engine model and, consequently, the calculation of fuel consumption, which is why it was not possible to proceed with the final optimization step.

Therefore, this chapter presents the results of the simulations performed with X-Plane for flight generation and training of the developed neural networks, while the optimization of vertical profiles remains an interesting topic for future research and for improving the fidelity of the model in supersonic scenarios.

6.1 MAIN CHALLENGES

The main difficulties encountered and the solutions adopted are listed below:

- **Anomalous thrust values:**
  The engine model provided excessive thrust values, so the throttle level corresponding to the maximum nominal thrust (32,370 lb per engine) was determined and the throttle was limited to this value during the simulation, which was 0.3636.

- **Horizontal instability of the aircraft:**
  To stabilize the aircraft, it was necessary to move the center of gravity (CG) 2.3 meters forward, entering the value directly into the code.

- **Calibration of PID controllers:**
  The calibration of the controllers was complicated by the dynamics of the Concorde, which differed from those of traditional commercial aircraft. After numerous attempts and grid searches, unconventional PID parameters were defined that were necessary to achieve stable control of the flight profile.

- **Code modifications:**
  Several parts of the code were adapted to handle the new model, including the calibration procedure. After these modifications, it was possible to start generating data at a rate of approximately 120 flights/hour, without simulation errors.

- **Simulation of afterburner deactivation:**
  To replicate the actual behavior of the Concorde, a 13–20% reduction in thrust was implemented at the moment of afterburner cut-off, which occurs after reaching a certain altitude.

- **Thrust behavior as a function of speed:**
  During data generation, it was observed that thrust increases with speed, which is expected behavior for turbojet engines and partially confirms the accuracy of the engine model.

6.2 GENERATED FLIGHTS

It was possible to generate approximately 4000 flights, and for each one, the simulator produced a .csv file containing an extensive set of variables recorded at each point in time: *Time, Distance, Altitude above ground, Latitude, Longitude, Throttle, Thrust, Thrust corrected, Engine N1, Engine N2, Ground speed, CAS, TAS, ROC, Acceleration, Flap Stick, θ, γ, σ, Alpha, vpath, hpath, Roll, Heading, CL overall, CD overall, Wind speed, Wind direction, Wind dir sin, Wind dir cos, Total weight, Segment, Flap 0, Runway friction, Climb CAS.*

As a first step, using a sample of 2000 flights, the flight paths graph shown in Fig.6.1 was created, which shows the trend of altitude above ground level as a function of distance traveled.

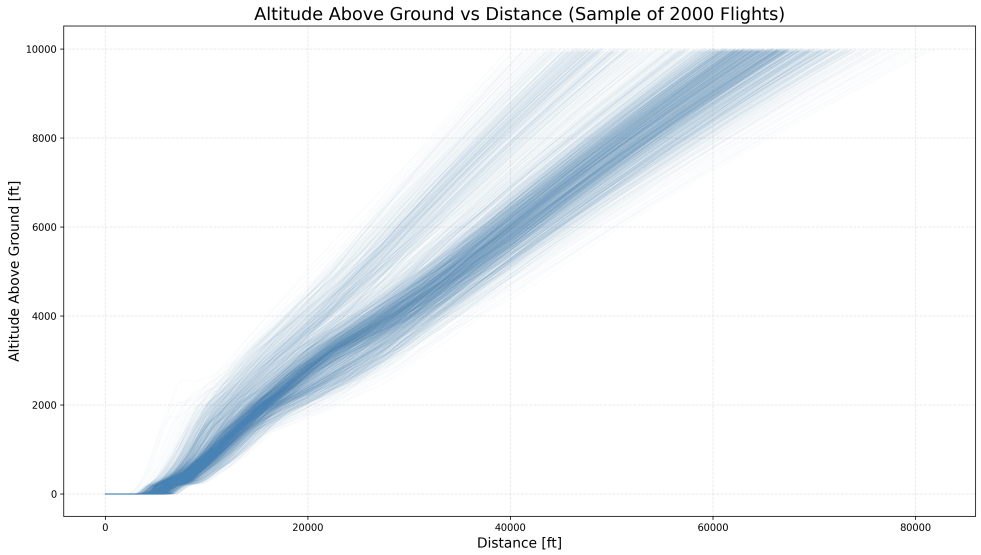

Figure 6.1: Generated flight paths

The following figures show the distribution of some fundamental parameters — CAS, TAS, Mach number and angle of climb — for each flight segment (Take-Off, Slow Climb, Acceleration and Fast Climb), using a boxplot representation. [1]

The trends in the graphs show that:

- The angle of climb [Fig. 6.2] is moderate at takeoff, increases during slow climb, and becomes more variable during acceleration, where trim changes are more frequent, then returns to stable during fast climb.
- The Mach number [Fig. 6.3] increases steadily throughout all phases, as a result of the increase in true airspeed and the decrease in the speed of sound with altitude.
- CAS [Fig. 6.4] is low and variable during takeoff, then stabilizes and increases during climb and acceleration phases until it becomes almost constant during the fast climb phase.
- TAS [Fig. 6.5] increases progressively from takeoff to climb, following the increase in altitude and thrust, and tends to stabilize in the final phases.

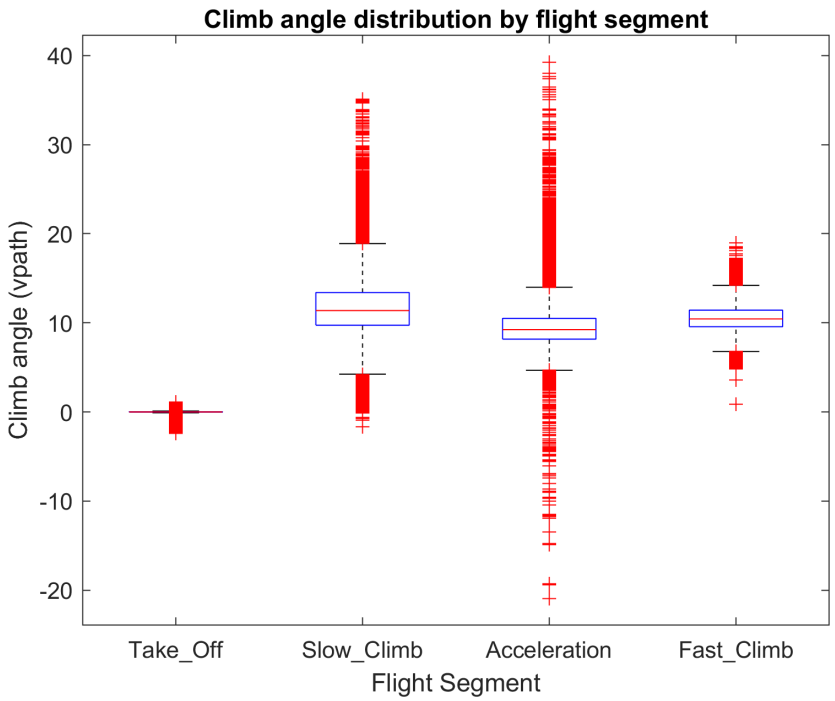

Figure 6.2: Climb angle distribution by flight segment

[1] In each boxplot, the blue box represents the central 50% of the data: the lower edge corresponds to the 25th percentile, the upper edge to the 75th percentile, while the central red line indicates the median. The vertical lines extending beyond the box are called whiskers and delimit the range of values that, although distant from the median, are still compatible with the expected behavior. Finally, the red symbols located outside the whiskers represent outliers, which are isolated measurements that deviate significantly from the rest of the distribution.

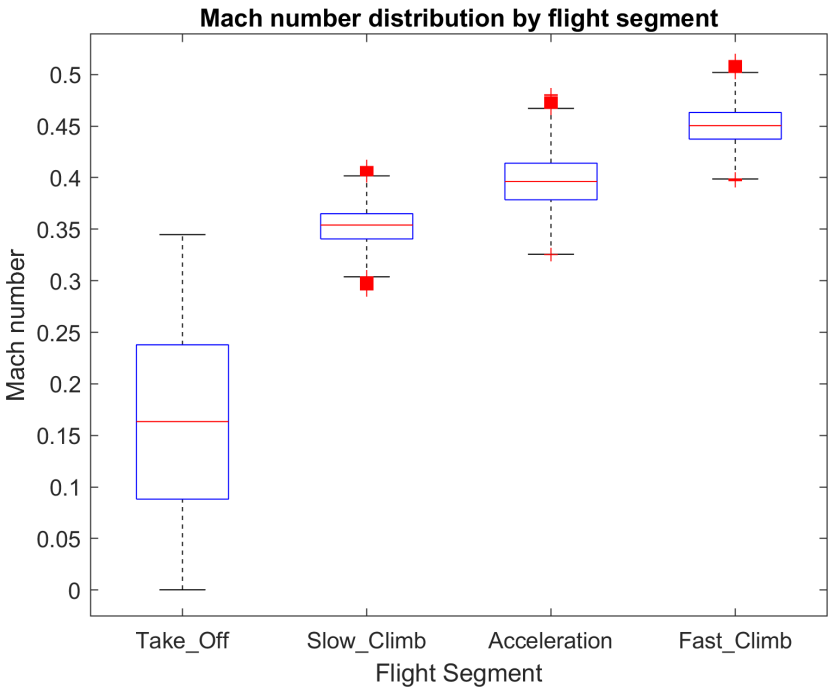

Figure 6.3: Mach number distribution by flight segment

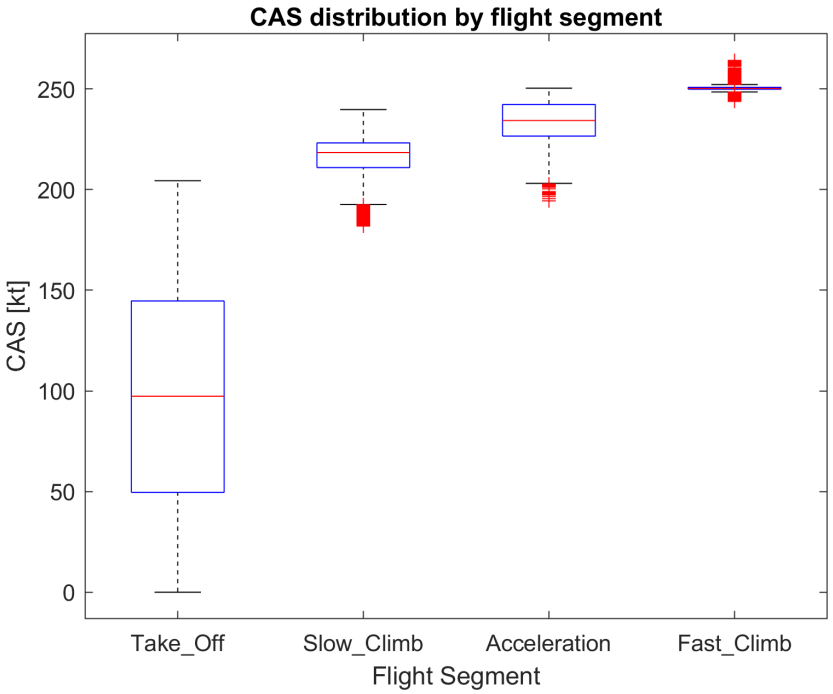

Figure 6.4: CAS distribution by flight segment

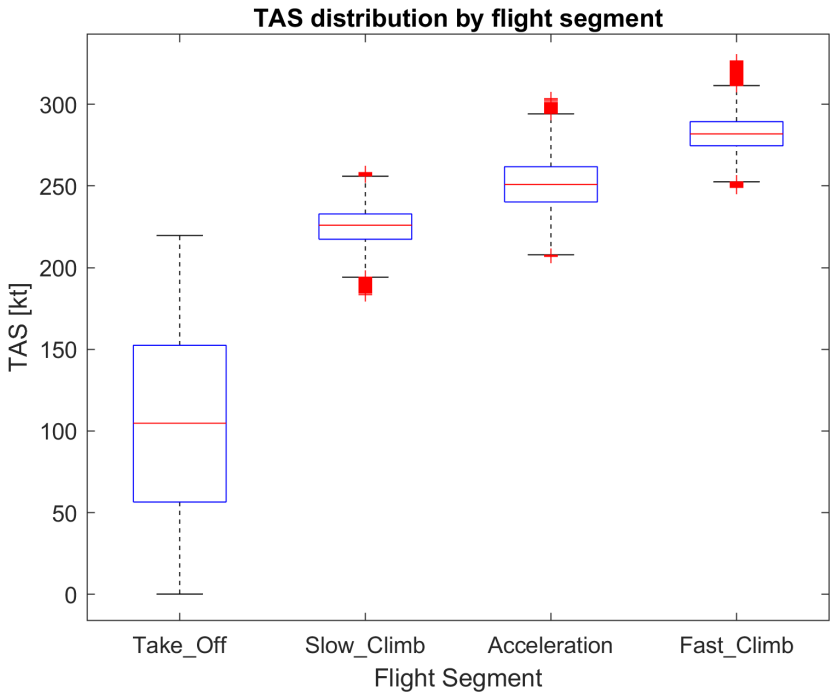

Figure 6.5: TAS distribution by flight segment

6.3 NEURAL NETWORK MODELS

The neural network models described in Section 4.3 were trained using a dataset consisting of 5186 flights, divided into 90% for training, 5% for validation and 5% for final testing, and the results obtained are shown below:

- **Weight model** [Fig. 6.6 , 6.7]

$$R^2 = 0{,}79570$$
$$\text{MAE} = 7412{,}43303 \text{ lb } (2.05\% \text{ of MTOW})$$
$$\text{Max err} = 21788{,}95592 \text{ lb}$$

- **Thrust model** [Fig. 6.8]
  To visually illustrate the behaviour of the model, a single sample flight was analysed, yielding:

$$R^2 = 0{,}98309$$
$$\text{MAE} = 479{,}2244 \text{ lbf}$$
$$\text{Max err} = 2035.37125 \text{ lbf}$$

  The estimated thrust curve closely follows that generated by X-Plane, even if with slight discrepancies.

In summary, both models showed a good level of accuracy and proved to be reliable tools for estimating weight and thrust along the climb profile.

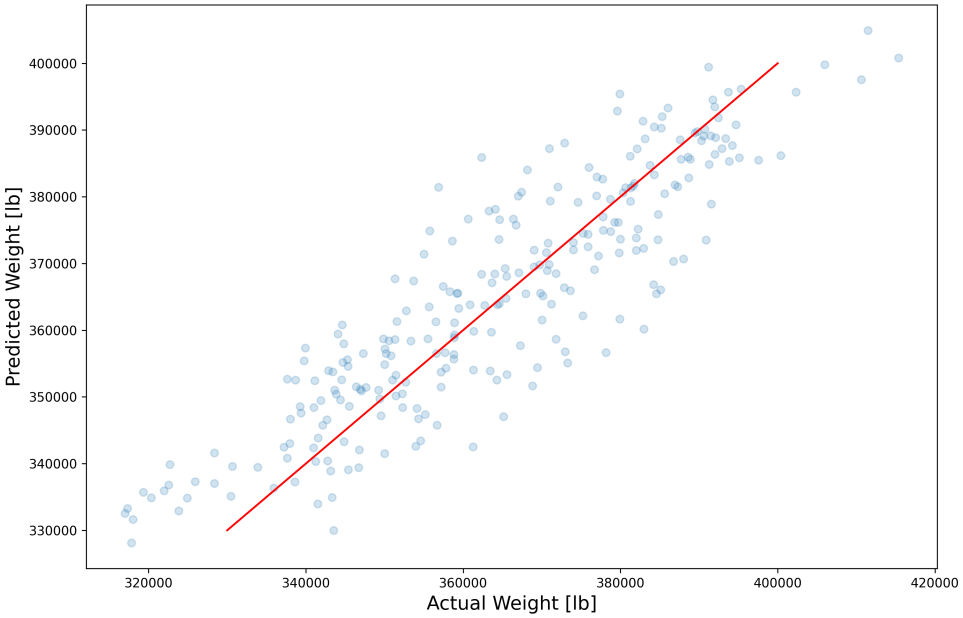

Figure 6.6: Weight model predictions

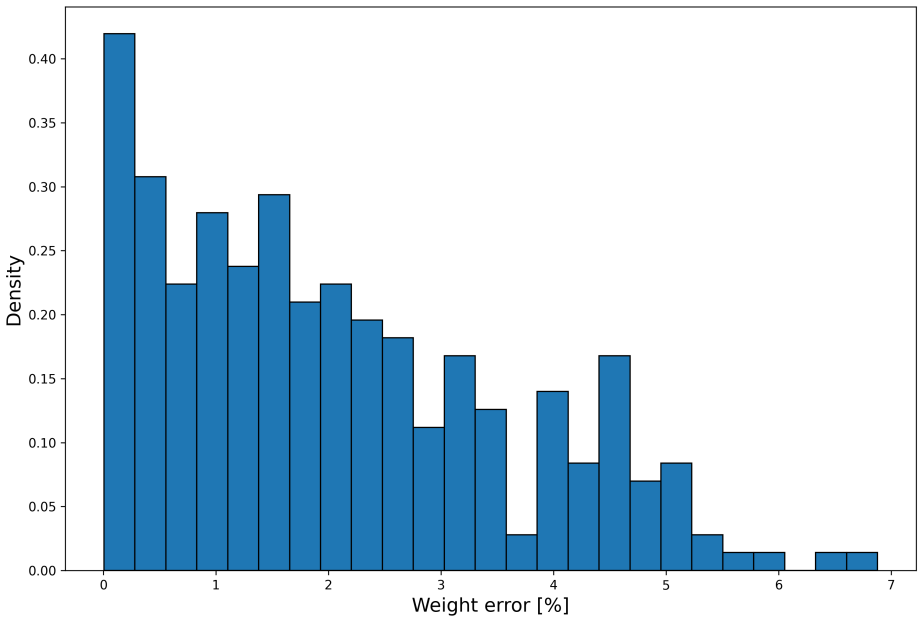

Figure 6.7: Weight prediction error distribution

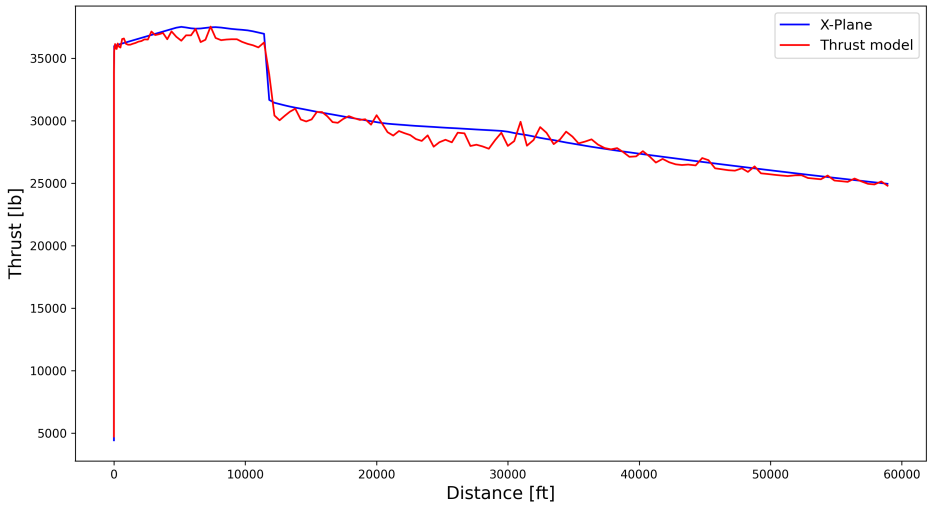

Figure 6.8: Thrust predictions for a single flight

Chapter 7

CONCLUSION

The results obtained highlight two main elements. On one side, the predictive models developed showed good reliability in estimating unobservable parameters such as weight and thrust, confirming the validity of the approach [2] based on the integration of flight simulators and neural networks for applications in real scenarios or scenarios lacking operational data.
On the other hand, the modeling of the supersonic aircraft highlighted some critical issues: the simulation required numerous adjustments and highlighted the need for further refinements, particularly in engine modeling and fuel consumption calculations.

Overall, the work carried out demonstrates that the combination of high-fidelity simulations and neural network-based predictive models is a promising approach for environmental assessments even in the absence of real data.
The optimization of vertical profiles and the complete assessment of environmental impact remain interesting objectives for future developments, together with improving model fidelity and including additional metrics such as nvPM and sonic boom.

Bibliography

[1] N. Viola and R. Fusaro. *Gestione dei rischi, costi e supporto logistico integrato dei sistemi aerospaziali*. Teaching material of the Politecnico di Torino, 2023/2024.

[2] Kiumars Askari and Michele Cremaschi. *Simulation-Based Prediction of Departure Aircraft Performance from Surveillance-like Data Using Neural Networks*. Aerospace, 2023.

[3] T. et al. Rotger. *A Review of the Current Regulatory Framework for Supersonic Civil Aircraft: Noise and Emissions Regulations*. Aerospace, 2024.

[4] Politecnico di Torino. *MOREandLESS: verso il futuro dell'aviazione civile supersonica*. `https://www.polito.it/ateneo/comunicazione-e-ufficio-stampa/comunicati-stampa/moreandless-verso-il-futuro-dell-aviazione-civile`, 2021.

[5] International Civil Aviation Organization. Annex 16 to the convention on International Civil Aviation: *Environmental Protection, Volume I — Aircraft Noise*, 2017.

[6] European Civil Aviation Conference. ECAC Doc 29, 4th edition: *Report on Standard Method of Computing Noise Contours around Civil Airports, Volume 1 — Applications Guide*, 2016.

[7] European Civil Aviation Conference. ECAC Doc 29, 4th edition: *Report on Standard Method of Computing Noise Contours around Civil Airports, Volume 2 — Technical Guide*, 2016.

[8] European Civil Aviation Conference. ECAC Doc 29, 4th edition: *Report on Standard Method of Computing Noise Contours around Civil Airports, , Volume 3 — Verification and Validation Guide*, 2016.

[9] Federal Aviation Administration. 14 CFR Part 36 — *Noise Standards: aircraft Type and Airworthiness Certification*, 2025.

[10] Federal Aviation Administration. 14 CFR Part 150 — *Airport Noise Compatibility Planning*, 2025.

[11] EUROCONTROL. *Aircraft Noise and Performance (ANP) Database*. `https://www.aircraftnoisemodel.org`, 2020.

[12] International Civil Aviation Organization. Annex 16 to the convention on International Civil Aviation: *Environmental Protection, Volume II — Aircraft Engine Emissions*, 2017.

[13] European Union Aviation Safety Agency. *ICAO Aircraft Engine Emissions Databank*. `https://www.easa.europa.eu/en/domains/environment/icao-aircraft-engine-emissions-databank`, 2025.

[14] Martin Schaefer and Sebastian Bartosch. *Overview on fuel flow correlation methods for the calculation of NOx, CO and HC emissions and their implementation into aircraft performance software*. Technical Report IB-325-11-13, DLR Institute of Propulsion Technology, 2013.

[15] B. et al. Owen. *Review: Particulate Matter Emissions from Aircraft*. Atmosphere, 2022.

[16] International Civil Aviation Organization. Doc 9889: *Airport Air Quality Manual*, 2020.

[17] International Civil Aviation Organization. Doc 8168: *Procedures for Air Navigation Services - Aircraft Operations, Volume I — Flight Procedures*, 2018.

[18] International Civil Aviation Organization. Icao circular 317 at/136: *Effects of PANS-OPS Noise Abatement Departure Procedures on Noise and Gaseous Emissions*, 2008.

[19] G. et al. Piccirillo. *Guidelines for the LTO Noise Assessment of Future Civil Supersonic Aircraft in Conceptual Design*. Aerospace, 2022.

[20] *Mach 2 Passenger Aircraft Using Bio-Fuels – Concorde Configuration*. Integrated Aerospace Systems Design – Team 1 Final Report, 2021/2022.

[21] Wikipedia. *Concorde*. `https://en.wikipedia.org/wiki/Concorde`, 2025.

[22] Heritage Concorde Team. *Technical Section*. `https://www.heritageconcorde.com/technical-section`, 2025.

[23] Davide Ferretto. *CS-1 Case Studies Definition*. Programme H2020 Deliverable D2.3, Politecnico di Torino, 2024.

[24] Laminar Research / X-Plane Developer. *Plane Maker Manual*. `https://developer.x-plane.com/manuals/planemaker/`.

[25] Danklaue. *PlaneMaker Tutorials* (youtube playlist). `https://www.youtube.com/watch?v=Os7O-uPhIHk&list=PL83BC4217746786FF`.

[26] Federal Aviation Administration. *Type Certificate Data Sheet No. E20EU: Olympus 593 Mk. 610-14-28*. Technical Report E20EU, U.S. Department of Transportation, 1981.

[27] Laminar Research / X-Plane Developer. *X-Plane Desktop Manual*. `https://x-plane.com/manuals/desktop/`.

[28] G. Bangga. *Comparison of Blade Element Method and CFD Simulations of a 10 MW Wind Turbine*. Fluids, 2018.

[29] International Civil Aviation Organization. Icao 9888: *Noise Abatement Procedures: Review of Research, Development and Implementation Projects*, 2010.

[30] Yoshua Bengio Ian Goodfellow and Aaron Courville. *Deep Learning*. MIT Press, 2016.

[31] Reza Paki, Kiumars Askari, and Michele Cremaschi. *Vertical profile noise optimization for aircraft departures using Flight Data Recorder-like data*. In SESAR Conference. ENV-ISA, 2024.

[32] Kalyanmoy Deb, Amrit Pratap, Sameer Agarwal, and T. Meyarivan. *A fast and elitist multiobjective genetic algorithm: NSGA-II*. IEEE Transactions on Evolutionary Computation, 6(2), 2002.